THE JOURNAL OF PHYSICAL CHEMISTRY B
A JOURNAL OF THE AMERICAN CHEMICAL SOCIETY

pubs.acs.org/JPCB

Article

Solvent Organization and Electrostatics Tuned by Solute Electronic Structure: Amide versus Non-Amide Carbonyls

Published as part of The Journal of Physical Chemistry virtual special issue "Biomolecular Electrostatic Phenomena".

Steven D. E. Fried, Chu Zheng, Yuezhi Mao, Thomas E. Markland,* and Steven G. Boxer*

Cite This: *J. Phys. Chem. B* 2022, 126, 5876−5886

Read Online

ACCESS | Metrics & More | Article Recommendations | Supporting Information

ABSTRACT: The ability to exploit carbonyl groups to measure electric fields in enzymes and other complex reactive environments by using the vibrational Stark effect has inspired growing interest in how these fields can be measured, tuned, and ultimately designed. Previous studies have concentrated on the role of the solvent in tuning the fields exerted on the solute. Here, we explore instead the role of the solute electronic structure in modifying the local solvent organization and electric field exerted on the solute. By measuring the infrared absorption spectra of amide-containing molecules, as prototypical peptides, and contrasting them with non-amide carbonyls in a wide range of solvents, we show that these solutes experience notable differences in their frequency shifts in polar solvents. Using vibrational Stark spectroscopy and molecular dynamics simulations, we demonstrate that while some of these differences can be rationalized by using the distinct intrinsic Stark tuning rates of the solutes, the larger frequency shifts for amides and dimethylurea primarily result from the larger solvent electric fields experienced by their carbonyl groups. These larger fields arise due to their stronger $p-\pi$ conjugation, which results in larger C═O bond dipole moments that further induce substantial solvent organization. Using electronic structure calculations, we decompose the electric fields into contributions from solvent molecules that are in the first solvation shell and those from the bulk and show that both of these contributions are significant and become larger with enhanced conjugation in solutes. These results show that structural modifications of a solute can be used to tune both the solvent organization and electrostatic environment, indicating the importance of a solute-centric paradigm in modulating and designing the electrostatic environment in condensed-phase chemical processes.

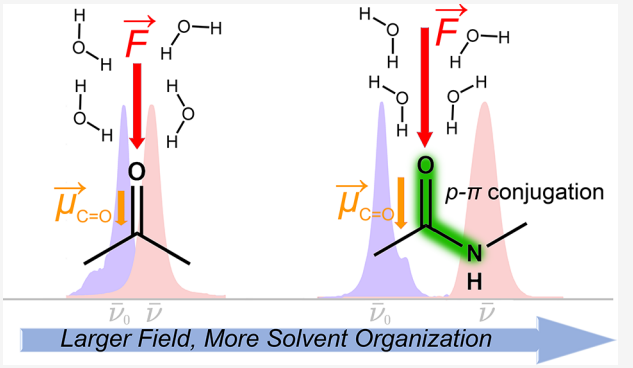

INTRODUCTION

Among fundamental chemical principles, the concept of solvation has long been a topic of significant research, playing a central role in disciplines such as supramolecular chemistry,[1] chemical reactivity,[2] macromolecular folding,[3] and colligative properties of solutions.[4] The molecular properties of both solute and solvent must be simultaneously considered to characterize the solvation process. These properties, which include the total molecular dipole moment and those of individual chemical bonds, the hydrogen-bonding donor or acceptor capability, polarizability, and molecular shape, will all influence the types of intermolecular forces between solute and solvent. Each of these interactions will in turn contribute to an overall electric field upon the solute, which can be probed spectroscopically by mapping from the observed frequency shifts by using the Stark effect, whether electronic[5,6] or vibrational.[7]

Solute−solvent interactions are frequently analyzed from the perspective of the solvent, where changes to solvent properties (e.g., polarity as characterized by the static dielectric constant, ε_s, or polarizability as characterized by the refractive index, η) can produce striking changes in a solute's absorption spectra, a phenomenon known as solvatochromism.[8,9] Solvatochromism for electronic transitions—the shift of the absorption spectrum due to changes in the solvent polarity—is widely used as a proxy to calibrate solvent polarity.[10] In the case of the vibrational Stark shifts, the changes in frequency can be connected to the electric field induced by the solvent by using

Received: May 5, 2022
Revised: July 4, 2022
Published: July 28, 2022

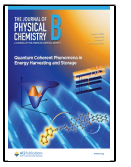

simulations to generate correlations between the observed frequencies and the calculated fields. This strategy has been successfully employed for probing solvent fields both around small molecules[11−13] and in complex and heterogeneous environments such as proteins.[14−18]

While solvatochromism studies have provided significant insights into the role played by the solvent in determining the electric fields experienced by the solute, these fields ultimately arise from the mutual interaction between the solvent and solute and thus also depend on the fields and structural ordering that the solute exerts on the solvent. These mutual interactions often require a compromise between solvent−solvent interactions and specific solvent−solute interactions such as those arising from charged or dipolar functional groups as well as steric effects.[19−21] Additionally, in some cases there can be a significant interplay between the solvent field and the electronic structure of the solute, such as in donor−acceptor polyenes where changes in solvent polarity lead to drastic changes in the bond-alternation pattern of the polyene.[22−24] Theoretical models that aim to mechanistically understand and predict how solutes direct solvent organization to produce spectroscopic frequency shifts originate with the reaction field model of Onsager[25] and have since been extended to more detailed self-consistent reaction fields[26,27] and more recent implicit solvent models.[28−32]

Here we elucidate how the molecular properties of solutes alter the electric fields they experience by investigating and contrasting molecules containing amide (amides and dimethylurea) and non-amide (ester, thioester, and ketone) carbonyls (Figure 1A) in a range of polar solvents. By employing

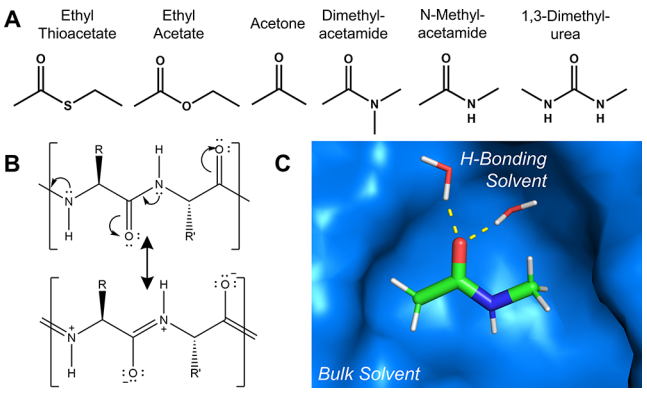

Figure 1. (A) Molecules used in this study. (B) Resonance within a peptide bond via $p-\pi$ conjugation increases the total dipole moment of the amide carbonyl through both charge separation and bond order reduction. (C) Carbonyl-containing solutes such as *N*-methylacetamide (shown with sticks) interact with solvent directly via hydrogen bonds (yellow) and by long-range electrostatic interactions with the bulk dielectric (blue). Both effects contribute to the electric field experienced by the solute carbonyl.

vibrational Stark and infrared (IR) spectroscopies and molecular dynamics (MD) simulations, we show that, of all the carbonyl-containing molecules studied, greater IR frequency shifts and larger fields are directed on carbonyls when nitrogen is included at one or both α-positions. The fields projected on these amide carbonyls are much larger due to the enhanced electron delocalization arising from the $p-\pi$ conjugation with the adjacent nitrogen atom (Figure 1B), which leads to enhanced carbonyl bond (C═O) dipole moments over non-amides and more pronounced solvent organization about them. The larger fields experienced by amides are important given their biochemical roles in proteins and other natural products,[33] including protein secondary structure determination[34,35] and the synthesis or hydrolysis of peptide bonds in ribosomes or proteases, respectively, which may involve catalysis through electrostatic stabilization of an oxyanion intermediate along the axis of the carbonyl.[36−39]

To gain insights into the underlying mechanism by which the $p-\pi$ conjugation effect in amides tunes the electric field on C═O, we then use electronic structure calculations to quantify the field contributions from solvent molecules in close contact with the solute (e.g., those in the first solvation shell or directly hydrogen bonded to the solute) and those from the bulk solvents, which are illustrated in Figure 1C. Using water as an example, we demonstrate the existence of a mechanism whereby stronger fields are mediated by increased number of hydrogen bonds (HBs) as well as greater organization of solvent molecules in the bulk, both of which contribute significantly to the field enhancement and increase simultaneously as the solute electronic structure is altered. By doing this, we provide insights into the relative importance of direct solute−solvent interactions and long-range dielectric effects in determining the electric field experienced by the solute and how these contributions change depending on the solute structure. This offers the opportunity to systematically understand the ways in which solute structures can be modified to tune the solvent organization and the resulting electrostatic environment for chemical processes in condensed-phase systems ranging from solutions to enzymes.

MATERIALS AND METHODS

Materials for Experimental Characterization. The carbonyl-containing compounds were acquired from the following sources: *N*,*N*-dimethylacetamide (DMA, 99.9%, Sigma-Aldrich), *N*-methylacetamide (NMA, 99%, Sigma-Aldrich), ethyl thioacetate (98%, Sigma-Aldrich), ethyl acetate (99.8%, Sigma-Aldrich), acetone (99.8%, Acros Organics), 1,3-dimethylurea (98%, Acros Organics). Solvents were purchased as follows: 2-methyltetrahydrofuran (2-MeTHF, >99%, Sigma-Aldrich), D_2O (100.0% atom D, Acros Organics), glycer(ol-d3) (99% atom D, Sigma-Aldrich), methanol (99.8%, Fisher Scientific), dimethyl sulfoxide (99.7%, Acros Organics), chloroform (99.9%, Acros Organics), dichloromethane (99.9%, Acros Organics), tetrahydrofuran (99.9%, Acros Organics), dibutyl ether (99%, Sigma-Aldrich), *n*-hexanes (99%, Sigma-Aldrich). All reagents were used without further purification.

Vibrational Solvatochromism. All infrared spectra were recorded by using a Bruker Vertex 70 FTIR spectrometer with a liquid-nitrogen-cooled mercury cadmium telluride (MCT) detector by using previously described methods.[14] A mountable liquid sample cell was constructed from two CaF_2 optical windows (0.75 in diameter, 0.25 in thickness, Red Optronics), separated by two semicircular Teflon (PTFE) spacers (25 and 50 μm thickness), to which 20 μL of sample solution (usually ∼10 mM, or ∼5 mM in the case of 1,3-dimethylurea in dibutyl ether) was added. Samples were purged within the instrument by a nitrogen flow for 5 min to remove atmospheric CO_2 and water vapor. Transmission spectra were then recorded by averaging 256 scans between 2000 and 1400 cm^{-1}, each time with 1 cm^{-1} resolution and aperture between 2 and 6 mm to maximize signal intensity without oversaturating the detector. Absorption spectra were

https://doi.org/10.1021/acs.jpcb.2c03095
J. Phys. Chem. B 2022, 126, 5876−5886

calculated by taking the negative logarithm of the transmission spectra and subtracting the spectrum of the blank. Experimental spectra for acetone and 1,3-dimethylurea were compared with previously collected FTIR spectra for dimethylacetamide, ethyl acetate, ethyl thioacetate, and *N*-methylacetamide by using similar methods.[17] Each solvatochromism measurement was repeated in triplicate, consistently by using three different orientations of the sample cell within the FTIR instrument. Frequencies of the carbonyl stretching band were selected by fitting Gauss−Lorentz curves to the relevant spectral region using the Levenberg−Marquardt algorithm. In cases of closely overlapping peaks, multiple Gauss−Lorentz curves were fitted, with a weighted sum taken based on their respective intensities to identify the ensemble average frequency position.

Vibrational Stark Spectroscopy. Vibrational Stark spectra for ethyl acetate, ethyl thioacetate, *N*-methylacetamide, and dimethylacetamide have been reported by Schneider and Boxer.[17] For this work, acetone and 1,3-dimethylurea were dissolved in glass-forming solvents as indicated with concentrations of 50 mM. Solutions were loaded into a sample cell composed of two offset CaF_2 windows (1 mm thickness, 12.7 mm diameter, TOCtek Photonics), each coated on the inner face with a 4.5 nm layer of nickel and separated by 26 μm Teflon spacers. Electrodes were connected to each window to convert the sample cell into a parallel-plate capacitor. The filled sample cell was quickly immersed in liquid N_2 in a custom-built cryostat,[40] and Stark spectra were recorded on a Bruker Vertex 70 FTIR spectrometer with fields of 0.5−1.8 MV/cm (applied voltages of ∼1.5−4.0 kV) from a Trek 10/10 high-voltage power amplifier using 1 cm^{-1} resolution and 64 scans apiece of field-on/off transmission spectra. Measurements were repeated with increasing fields to ensure that the intensity of the Stark spectrum scales linearly with the square of the field strength as expected for an isotropic, immobilized sample.[41]

The linear Stark tuning rate was determined as previously described by numerically fitting the zeroth, first, and second derivatives of the best-fit Voigt profile of the experimental absorbance spectrum to the Stark spectrum.[41] This analysis assumes an isotropic, immobilized sample and that the angle (ζ) between $\Delta\vec{\mu}_{C=O}$ and the transition dipole is zero; the experimentally set angle (χ) between the incident light polarization and the external electric field direction was 90° as previously described (see the Supporting Information, section I).[41] In cases where overlapping peaks were observed (e.g., where both hydrogen-bonding and non-hydrogen-bonding species occur), the derivative contributions were determined from the full absorbance spectrum in the spectral region of interest unless otherwise noted. Note that while the applied electric field ($\vec{F}_{ext}$) is known accurately from the applied voltage and separation of the electrode, the actual field experienced by the probe ($\vec{F}_{local}$) differs from this value and needs to be adjusted by a local field correction factor (f), i.e., $\vec{F}_{local} = f\vec{F}_{ext}$.[41,42] While the exact value of the local field factor is not known (and is treated here as a scaler), it is expected to have a value between 1 and 2 for carbonyls.[7,13,16,43] As such, the Stark tuning rates are reported in terms of $|\Delta\vec{\mu}_{C=O}|f$; this will be discussed in further detail with the results.

Molecular Dynamics (MD) Simulations. The carbonyl-containing solute molecules were parametrized using Gaussian 16[44] and AmberTools20.[45] The molecules were constructed in GaussView and then geometry-optimized using DFT at the B3LYP/6-311++G(2d,2p) level.[46,47] Optimized solute structures were input into the Antechamber program of AmberTools and parametrized using the General Amber Force Field (GAFF)[48] and the AM1-BCC method[49] to assign fixed atomic charges. Organic solvent parameters were taken from Caleman et al.,[50] while for water the TIP3P model[51] was employed. All MD simulations were set up and performed in GROMACS 2018.[52,53] Each solute was solvated in GROMACS via *gmx solvate* using the benchmarked densities from Caleman et al.[50] in a cubic periodic box of length 40 Å.

The MD simulations were performed with periodic boundary conditions, where long-range electrostatics was treated by particle-mesh-Ewald (PME) with a 1 nm real-space cutoff. The system was first energy-minimized, prior to equilibration in the NVT ensemble for 200 ps at 300 K followed by 200 ps in the NPT ensemble at the same temperature and a pressure of 1 bar. Temperature coupling was controlled with a stochastic velocity-rescaling thermostat[54] and pressure via the Parrinello−Rahman barostat.[55] MD production runs (in NPT) were performed for a total of 1 ns, with snapshots of the forces and positions recorded every 200 fs, producing a total of 5000 snapshots per trajectory. For the calculation of radial distribution functions, the positions were recorded every 2 fs.

Electric Field Calculations. Electric fields acting on the solute carbonyl groups were calculated by using both classical force fields and electronic structure methods at the DFT level. In the first approach, the electric field vectors on the carbon and oxygen atoms were obtained from the electrostatic forces acting on them in each snapshot employing a previously established approach.[14] The total electric field on the carbonyl group was then calculated by averaging the projection of each atom's field vector along the C═O bond direction. Repeating this for each snapshot, the ensemble-averaged value is reported for each solute−solvent combination.

The electric field calculations at the DFT level were performed on the selected MD frames for all six solutes in water by using the Q-Chem 5.4.2 software package.[56] The MD frames were first sorted based on the number of hydrogen bonds formed between the carbonyl group and the surrounding water molecules, and then 100 frames were randomly selected from each group on which the electronic structure calculations were performed (unless the group contained fewer than 100 frames, in which case all frames were used). The detailed procedure for DFT-based electric field calculations has been elaborated elsewhere.[57] In brief, we first generated truncated solute−solvent clusters with a cutoff radius of 7 Å; that is, the center-of-mass of each included solvent molecule is within 7 Å of at least one of the solute atoms. We then employed the Subsystem Projection Atomic Orbital Decomposition (SPADE)[58] method to partition the electron density of the entire solute−solvent system, based on DFT calculations at the B3LYP/6-31+G(d) level. The electron density assigned by this partitioning to the solvent part of the system, together with the solvent nuclei, was then used to calculate the electric field vectors on the carbon and oxygen atoms and then the electric field on the carbonyl group.

Hydrogen-Bond Analysis and Decomposition of Solvent Electric Fields. The number of HBs between solute and solvent, plus the angular and distance distributions of those HBs for each solute, was determined by using the *gmx hbond* function based on a widely used geometrical criterion for HBs:[59] for the protic solvents (water and methanol), an HB between a solvent O−H group and the solute carbonyl group

https://doi.org/10.1021/acs.jpcb.2c03095
J. Phys. Chem. B 2022, 126, 5876−5886

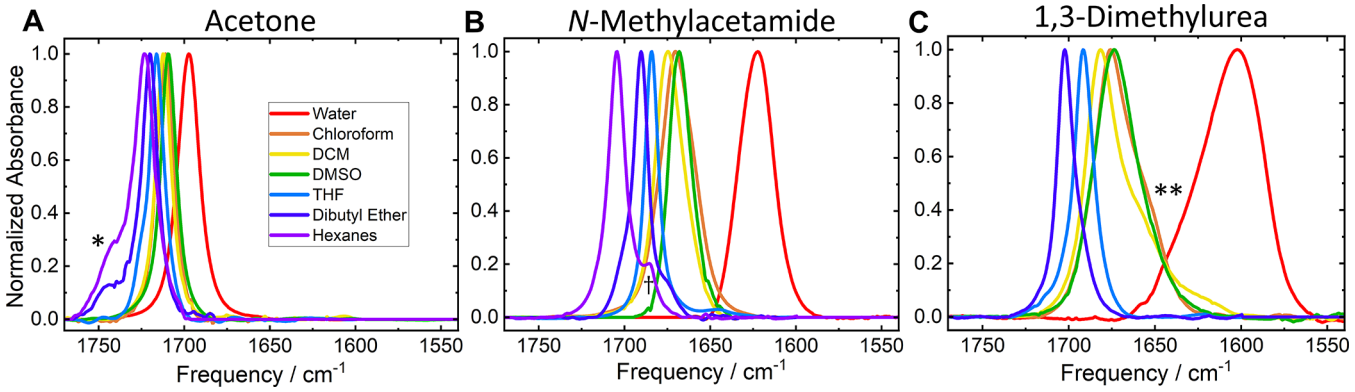

Figure 2. FTIR spectra of (A) acetone, (B) *N*-methylacetamide, and (C) 1,3-dimethylurea show increasing frequency shifts in more polar solvents. Note that the *x*-axis scale (in cm^{-1}) is the same in all three panels, making it immediately clear that much larger spectral shifts with solvent polarity are observed for 1,3-dimethylurea than for acetone. Solvents range in polarity from hexanes to water for acetone and *N*-methylacetamide and from dibutyl ether to water for 1,3-dimethylurea. Observed shoulder peaks arise due to combination modes (CC stretch + CO in-plane bend) in acetone (∗) or dimerization in nonpolar solvents for *N*-methylacetamide (†). Peak asymmetries such as those observed for 1,3-dimethylurea in polar solvents (∗∗) may arise from heterogeneities in the solvent environment around the solute that can form multiple H-bonds.[17]

is defined to occur when the $O_{Solvent}\cdots O_{Solute}$ distance is within 3.5 Å and the $H-O_{Solvent}-O_{Solute}$ angle is below 30°. HB interactions to chloroform were identified similarly by a $C_{Solvent}\cdots O_{Solute}$ distance within 4.0 Å, accounting for the longer interaction distances, and a $H-C_{Solvent}-O_{Solute}$ angle below 30°. The HB cutoff distances chosen for OH-containing solvents (water and methanol) and chloroform both approximately correspond to the distances to the first minimum of the radial distribution functions (RDFs) calculated from the MD simulations.

In water, we quantified the respective contributions from solvent molecules in the first solvation shell (those whose oxygen atoms, O_w, are within 3.5 Å of the carbonyl oxygen, O_c) and from those outside (i.e., bulk solvents). These contributions are termed the *inner-* and *outer-shell* contributions to the field, respectively, throughout this paper, and they were obtained from DFT-based electric field calculations with either the outer- or inner-shell water molecules removed from the solute−solvent clusters. An additional nonadditive component was then evaluated by subtracting these two contributions from the total electric field acting on C═O, which primarily reflects the effect of mutual polarization between the inner- and outer-shell water molecules. A similar analysis was also performed to determine the field contributions from HB and non-HB water molecules, where the solvent water molecules were categorized based on both the distance and angular criteria for HBs.

RESULTS AND DISCUSSION

Experimental Observation of Stronger Solvent-Induced Frequency Shifts for Amides versus Non-Amides. Figure 2 shows the FTIR spectra obtained for several carbonyl-containing molecules, as an extension of the previous results of Schneider and Boxer (Supporting Information Tables S1−S6).[17] From this it is clear that the relative frequency shifts for the amide-containing molecules (*N*-methylacetamide and 1,3-dimethylurea) are much greater than those observed for acetone: the C═O stretch mode of acetone shifts by only 25 cm^{-1} upon going from the least (hexane) to most polar (water) solvent studied, while that of 1,3-dimethylurea shifts by ∼100 cm^{-1}. This is consistent with the previous results showing a similar disparity when comparing the C═O frequency shifts observed for dimethylacetamide to those of ethyl acetate and ethyl thioacetate.[17] We further note a general broadening of the spectra in more polar solvents, which is more significant in the case of 1,3-dimethylurea while to a lesser extent in acetone.

To uncover the origin(s) of these striking observations, we consider the interpretation of these results within the framework of the first-order vibrational Stark effect (VSE), which predicts a linear response of infrared absorption frequency to the electric field experienced by the probe oscillator along the axis of its vibrational mode.[7,12] This is an intrinsic result of the anharmonicity of the oscillator, where the equilibrium bond length d increases upon the transition from the ground to first excited vibrational state. For a polar oscillator with charge separation q, this will entail a change in dipole from $\vec{\mu}_0 = q\vec{d}$ to $\vec{\mu}_1 = q(\vec{d} + \Delta\vec{d})$. Note that, in addition to the internal energy of the molecule itself, the electric field arising from a molecule's environment will interact with the oscillator dipole moment to change the total energy in both the ground and excited vibrational states. Hence, in the presence of a solvent-induced electric field $\vec{F}$, the IR frequency for a carbonyl will change by $\Delta\bar{\nu}_{C=O} = -\Delta\vec{\mu}_{C=O}\cdot\vec{F} = -|\Delta\vec{\mu}_{C=O}|F_{C=O}$ due to the interaction of the carbonyl difference dipole $\Delta\vec{\mu}_{C=O} = \vec{\mu}_1 - \vec{\mu}_0$ with the field projected onto the carbonyl ($F_{C=O}$). Because the carbonyl dipole typically increases upon excitation, such an interaction is energetically favorable when the field from a polar solvent is aligned with the bond direction, leading to a red-shift in the vibrational absorption spectrum. Electric fields along the carbonyl can thus be proportionally mapped onto changes in its vibrational frequency according to the Stark tuning rate $|\Delta\vec{\mu}_{C=O}|$. We see that there are two primary factors that can explain the significant difference in $\Delta\bar{\nu}_{C=O}$ for various carbonyls, namely the Stark tuning rate $|\Delta\vec{\mu}_{C=O}|$ as a molecular property associated with the solute electronic structure and the solvent-induced electric field exerted on the carbonyl bond ($F_{C=O}$). To characterize which property (or combination thereof) is at work in the structure-dependent variation in frequency shifts, we use a combination of experimental and computational means to separately assess both $|\Delta\vec{\mu}_{C=O}|$ and $F_{C=O}$ as well as the factors leading to their variations.

https://doi.org/10.1021/acs.jpcb.2c03095
J. Phys. Chem. B 2022, 126, 5876−5886

Table 1. Vibrational Stark Tuning Rates for Carbonyl-Containing Compounds in Frozen Glasses at 77 K Compared to Solvatochromism Values[a]

solute	VSS $\lvert\Delta\mu_{C=O}\rvert f$ in $cm^{-1}/(MV/cm)$	estimated VSS $\lvert\Delta\mu_{C=O}\rvert$ with $f = 2$ in $cm^{-1}/(MV/cm)$	solvatochromism $\lvert\Delta\mu_{C=O}\rvert$ in $cm^{-1}/(MV/cm)$	apparent f (VSS/solvatochromism)
ethyl thioacetate	1.47 ± 0.01†	0.74	0.55 ± 0.02	2.7 ± 0.1
ethyl acetate	1.15†	0.58	0.61 ± 0.04	1.9 ± 0.1
acetone	0.74	0.37	0.31 ± 0.01	2.39 ± 0.08
dimethylacetamide	1.25†	0.63	0.68 ± 0.06	1.8 ± 0.2
dimethylacetamide in ethanol	1.26†	0.63		
N-methylacetamide	1.30†	0.65	0.75 ± 0.02	1.73 ± 0.05
N-methylacetamide in 1:1 glycer(ol-D_3)−D_2O	1.30 ± 0.01†	0.65		
1,3-dimethylurea	1.24	0.62	1.02 ± 0.03	1.22 ± 0.04

[a]Values reported originally in this work or (for †) in ref 17. Frozen glass solvents for VSS are 2-methyl tetrahydrofuran unless stated otherwise. The error intervals for solvatochromism Stark tuning rates are standard errors of the field-frequency linear regression.

We first consider the role of the Stark tuning rate $\lvert\Delta\vec{\mu}_{C=O}\rvert$ in determining the observed larger amide frequency shifts by performing vibrational Stark spectroscopy (VSS) experiments, where an external electric field is applied to an isotropic immobilized sample in a frozen glass. The resulting changes in the absorption spectra can be used to calibrate the Stark tuning rate.[41] For each molecule investigated by VSS, the Stark spectra we measured are almost entirely dominated by the second derivative of the absorbance spectrum, from which we obtain $\lvert\Delta\vec{\mu}_{C=O}\rvert f$, where f is the local field factor that accounts for the difference between the electric field experienced in the frozen glass and the field applied externally to the sample (see the Supporting Information, section I).[7,41,60] For carbonyls, the local field factor f is thought to be around 2 in value.[7] However, the exact value may vary slightly depending on the solute, accounting for the differences between the $\lvert\Delta\vec{\mu}_{C=O}\rvert$ values determined from solvatochromism and those estimated from VSS by using $f = 2$ (see the Supporting Information, section 1). The results of the VSS measurements ($\lvert\Delta\vec{\mu}_{C=O}\rvert f$) for each compound are summarized in the second column of Table 1, where the results from this work for acetone and 1,3-dimethylurea (Figures S1 and S2) are combined with those obtained previously by Schneider and Boxer.[17] The very similar values of $\lvert\Delta\vec{\mu}_{C=O}\rvert f$ shown in Table 1 for NMA in 2-MeTHF and 1:1 glycer(ol-d_3)−D_2O (both at 1.30 $cm^{-1}/(MV/cm)$) and those for DMA in 2-MeTHF and ethanol (1.25 vs 1.26 $cm^{-1}/(MV/cm)$) suggest that the local field factor changes negligibly with the glass-forming solvent used, at least in these cases.

Assuming that the variation in f across these solutes is relatively small, one can use the variations in $\lvert\Delta\vec{\mu}_{C=O}\rvert f$ among these molecules to help explain the observed differences in solvent-induced frequency shifts in Figure 2, which can further be compared with the independently obtained results in the following section by using vibrational solvatochromism (Figures S3 and S4). In particular, the $\lvert\Delta\vec{\mu}_{C=O}\rvert f$ value of acetone, 0.74 $cm^{-1}/(MV/cm)$, is significantly lower than that of the other molecules, consistent with the observation that its frequency shift due to solvent field is the lowest. On the other hand, variations in $\lvert\Delta\vec{\mu}_{C=O}\rvert f$ alone cannot fully explain the differences in frequency shift between the various carbonyl-containing molecules. While $\lvert\Delta\vec{\mu}_{C=O}\rvert f$ for acetone is always between 1/2−2/3 of that of the other molecules, its solvent-induced frequency shifts are substantially smaller (1/4−1/3 of the others). The amide group has a particularly striking effect: while the amides, ester, thioester, and dimethylurea all have comparable $\lvert\Delta\vec{\mu}_{C=O}\rvert f$ values (Table 1), the solvent-induced frequency shifts of amides, and particularly dimethylurea, are significantly larger, suggesting that their intrinsic Stark tuning rates alone are unable to account for their large frequency shifts. Variations in the Stark tuning rates of these carbonyls due to solvent-induced bond polarization are expected to be insignificant as well.[61,62] Therefore, differences between the solvent electric fields experienced by the amide and non-amide carbonyls should play an even more important role in accounting for the larger solvatochromic shifts of the former, and next we combine the vibrational solvatochromism data and molecular dynamics simulations to investigate how the C=O frequency of each solute varies with the solvent electric field.

Characterizing Stark Tuning Rates Using Vibrational Solvatochromism and MD Simulations. To understand how the magnitude of electric field on the carbonyl ($F_{C=O}$) varies in different solute−solvent systems, we performed MD simulations of the six solutes in Table 1 in a wide range of solvents of low (hexane) to high (water) polarities and obtained the ensemble-averaged values of $F_{C=O}$ (i.e., $\langle F_{C=O}\rangle$). The variation in the electric fields for the non-amide (Figure 3A) and amide (Figure 3B) carbonyls as the solvent polarity is increased provides significant insights into the observed differences in frequency shifts. From non-amide to amide solutes, the fields projected on C=O nearly double in size, with some variation in different solvents. Note that the greater relative changes in $\langle F_{C=O}\rangle$ for some solvent−solute systems versus others indicate the limitations of the simple picture afforded by Onsager's reaction field model; that is, it does not consider the local interactions probed by vibrational features, which are particularly important for solute interactions with protic solvents.[63]

The magnitudes of the fields obtained from simulations (Table S7) show a strong linear correlation with the experimentally observed peak frequency shifts (Figure 3), in keeping with the first-order VSE. The slope in each case gives another estimate for the apparent Stark tuning rates ($\lvert\Delta\vec{\mu}_{C=O}\rvert$), and these values are in good agreement with the VSS values estimated assuming $f \approx 2$ with the exceptions of ethyl thioacetate and 1,3-dimethylurea (comparing the third and fourth columns in Table 1). The slopes obtained from least-squares fitting undergo no significant changes with the inclusion or exclusion of water, indicating the robustness of carbonyl probes for both protic and aprotic environments (Figure S5 and Table S8).[14] Note that variations in $\lvert\Delta\vec{\mu}_{C=O}\rvert$ for these two molecules account for the observed differences in spectral broadening (Figure 2). While each of the carbonyls experiences more variable solvent electric fields in polar

https://doi.org/10.1021/acs.jpcb.2c03095
J. Phys. Chem. B 2022, 126, 5876−5886

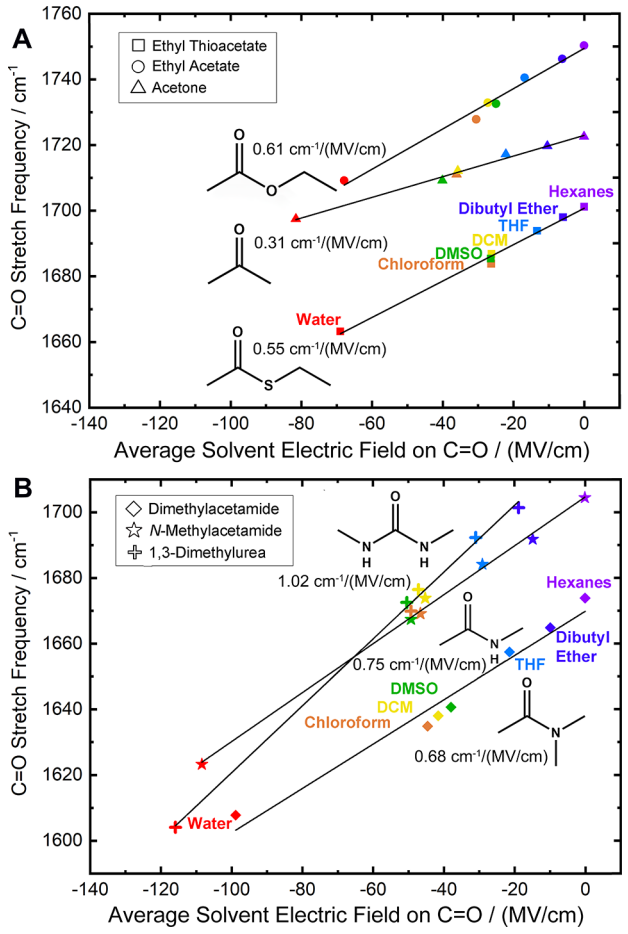

Figure 3. Field−frequency correlation plots for (A) smaller-field carbonyl-containing molecules (ester, thioester, ketone) and (B) larger-field amide and dimethylurea molecules. Here experimentally observed frequencies from FTIR measurements are plotted against the average values of $F_{C=O}$ (i.e., $\langle F_{C=O} \rangle$) calculated by using classical force fields in a broad range of solvents. Slopes of the linear correlations (apparent Stark tuning rates $|\Delta\vec{\mu}_{C=O}|$) are provided next to each line, which are characteristically different for acetone and 1,3-dimethylurea (0.31 and 1.02 $cm^{-1}/(MV/cm)$, respectively).

solvents because of the increased interaction strength and heterogeneity, the similar field variances (Table S9) map to wider line broadening in the IR spectra for solutes of larger Stark tuning rates, as shown by the contrast between 1,3-dimethylurea and acetone. For the other four carbonyls, including both amides, the ester, and thioester, the Stark tuning rates obtained from both VSS (using $f = 2$) and solvatochromism data consistently fall in the range 0.55−0.75 $cm^{-1}/(MV/cm)$. The smaller change in $|\Delta\vec{\mu}_{C=O}|$ across these four solutes (i.e., within a factor of 1.35) compared to the variation in solvatochromic shifts going from hexane to water (differing by a factor of up to 1.75) suggests that the amide-containing solutes can induce solvent organization about them to enhance the electric field that stabilizes the carbonyl.

Increased Solvent Organization around Amide Solutes and the Effects on Calculated Electric Fields. We now aim to correlate the structural properties of the solvents and solutes with the observed electric fields. As shown in Figure S6, the first solvation peak in the radial distribution functions (RDFs) of each simulated solvent about the solute carbonyl oxygen is notably more pronounced for the amides and 1,3-dimethylurea than for the other solutes, while the peak position, r_{max}, stays essentially invariant for a given solvent regardless of the solute (Figure 4A and Figure S6). This holds

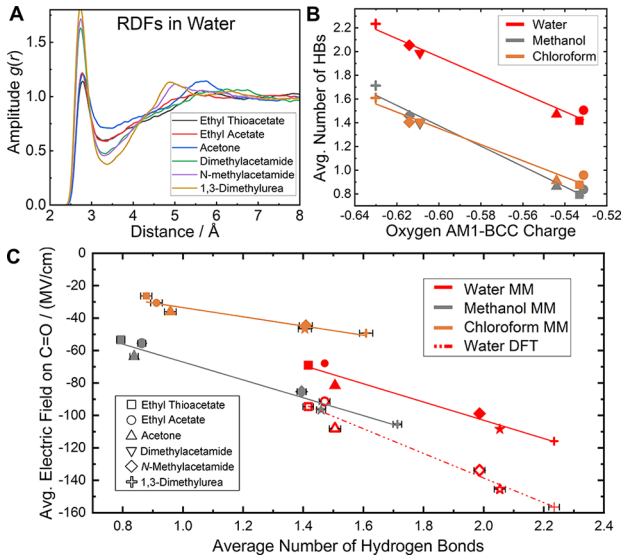

Figure 4. (A) Radial distribution functions (RDFs) describing distance distribution between O_w in water and the carbonyl oxygen in six various solutes. (B) Linear correlation between the AM1-BCC partial charges on the carbonyl oxygen (O_c) used in the simulations and the average number of HBs formed to the carbonyl for the same six solutes in three HB-forming solvents: water, methanol, and chloroform. (C) Linear correlation between the average electric field experienced by the solute carbonyl and the average number of HBs it forms in the three HB-forming solvents. The electric fields are calculated by classical molecular mechanics (MM) force fields for each of the solvents and, additionally, by DFT in the case of water.

for all three solvents studied here that can form HBs with the carbonyls: water, methanol ($r_{max} \approx 2.7$ Å for both), and chloroform ($r_{max} \approx 3.3$ Å). The similar first solvation peak positions for these solutes in each solvent but distinct amplitudes suggest that the number of HBs (n_{HB}) formed by each solute carbonyl toward HB-donor solvents (Table S10) may account for the differences in the electric fields they experience. We confirm this trend by demonstrating the linear correlation between the ensemble-averaged value of n_{HB} ($\langle n_{HB} \rangle$) and the magnitude of $\langle F_{C=O} \rangle$ in three solvents: water, methanol, and chloroform. The variation in $\langle n_{HB} \rangle$ for the different solutes can be seen to correlate strongly with the AM1-BCC partial charges on their carbonyl oxygens that were assigned via AmberTools for the MD simulations (Figure 4B).[49] The higher charges (Table S11) and hence larger bond dipoles (Table S12) of the amide carbonyls, as obtained from DFT calculations in a vacuum and in the force fields employed (where the fixed charges were also assigned based on electronic structure calculations), arise from the larger extent of $p-\pi$ conjugation in these molecules. We also find that DFT predicts higher charges on the carbonyl oxygen in solvated environments (Table S13) with a very small difference in the amount of charge transferred to the solvent water (Table S14), allowing the highly dipolar amide carbonyls to induce stronger organization of the nearby solvent molecules. As shown in Figure 4, the greatest changes in $\langle n_{HB} \rangle$ and $\langle F_{C=O} \rangle$ occur between the ketone (acetone) and the first amide (DMA) and to a lesser extent between the amides and 1,3-dimethylurea

https://doi.org/10.1021/acs.jpcb.2c03095
J. Phys. Chem. B 2022, 126, 5876−5886

(the latter has one additional sp^2-nitrogen in conjugation with the carbonyl). In the case of ethyl acetate and ethyl thioacetate, the conjugation effects are insignificant due to the high electronegativity of oxygen and higher shell number of sulfur, respectively, leading to lesser changes to the polarity of their carbonyl groups.

The results in Figure 4 thus indicate that the substantial increase in $\langle n_{HB} \rangle$ (e.g., from 1.42 for ethyl thioacetate to 2.23 for 1,3-dimethylurea in water) leads to a larger solvent electric field on the carbonyls of these solutes. On the other hand, as shown in the correlations between $\langle n_{HB} \rangle$ and $\langle F_{C=O} \rangle$ for each individual solute within a single MD trajectory (Figures S7 and S8), the electric fields will still be on average negative (stabilizing) for those frames where $\langle n_{HB} \rangle = 0$, indicating a sizable contribution that does not just arise from the HB solvent molecules in the first coordination shell. To further investigate the molecular details, we then employ electronic structure calculations to decompose the total solvent electric fields into direct HB and bulk components and demonstrate how each of them depends on n_{HB}.

Decomposing the Solvent Electric Fields Experienced by Carbonyls in Different Hydrogen-Bonding Environments. We employed DFT calculations to quantify the respective contributions to the electric fields on solute carbonyls ($\langle F_{C=O} \rangle$) in water from solvent molecules within the first coordination shell ($r_{O_wO_c} \leq 3.5$ Å, where O_w and O_c denote the water and carbonyl oxygens, respectively) and from those outside ($r_{O_wO_c} > 3.5$ Å) in different HB environments as characterized by using the n_{HB} value of each configuration. Note that DFT gives larger fields than those obtained from the employed force field (see the red solid and patterned lines in Figure 4C) because of its ability to capture phenomena like solvent polarization. Nevertheless, because DFT systematically increases the field strength for each solute−solvent system by ∼30 MV/cm, it only slightly affects the apparent Stark tuning rates which depend only on the slopes of the field-frequency correlations. Figures 5A and 5B show the variations of the inner- and outer-shell field contributions with n_{HB}, respectively. The magnitudes of the inner-shell contributions increase approximately linearly with n_{HB}. For each solvent, slight curvature toward saturation of field strength with higher n_{HB} (3 and 4) arises from the decrease in the field contribution per HB as more HBs are formed due to the increasingly crowded first coordination shell (i.e., shift of the $r_{O_wO_c}$ distribution to longer distances for configurations with larger n_{HB}, see Figure S9 and Table S15). While the inner- and outer-shell waters together contribute to ∼95% of the total field, the remaining contribution arises from the mutual polarization between the solvation shells, which makes the field on C═O even more stabilizing (Figure 5A).

Figure 5C shows the average contributions from the inner- and outer-shell water molecules as well as the mutual polarization between them for all six solutes, which are obtained by weighting the $\langle F_{C=O} \rangle$ values of each solute (as shown in Figure 5A,B) by their characteristic population of each n_{HB} group (Table S10). While for all the solutes the inner-shell waters make the largest contribution to the field accounting for 68−81% of the total, there is also a significant contribution from the outer shells ranging from 14% to 27%. This notable electric field contribution from the outer shell may likewise extend to functionally important electrostatic interactions in proteins, considering both the HB interactions

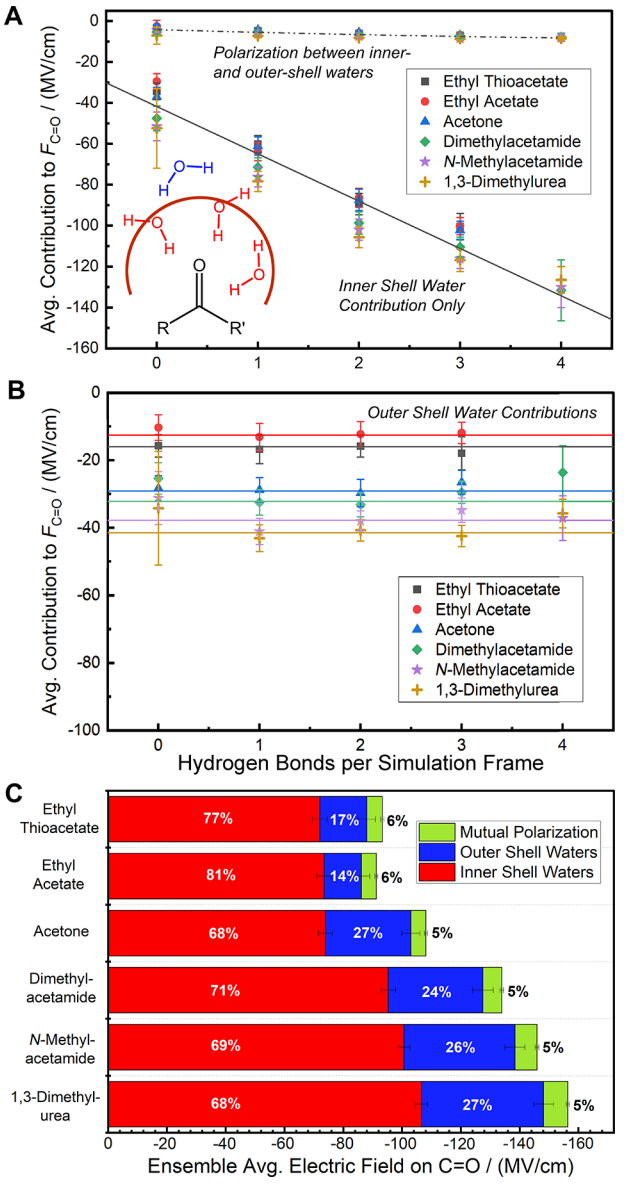

Figure 5. Separation of contributions to the overall electric field on carbonyls $\langle F_{C=O} \rangle$ for six solute molecules based on DFT calculations. (A) Electric field contributions arising from waters in the first solvation shell (up to 3.5 Å from the carbonyl oxygen, solid line) and the component of the overall field describing the polarization between inner- and outer-shell waters (patterned line), where linear models are fitted through the plotted points (average fields from up to 100 snapshots for each n_{HB}) collectively to guide the eye. (B) Field contributions from outer-shell solvent water molecules, where the solid lines indicate ensemble-averaged outer-shell contributions to the field on each solute. (C) Ensemble-averaged electric field for each of the six carbonyl-containing solutes, with the absolute strengths and percentage weights of the inner-shell, outer-shell, and mutual polarization components depicted.

in the short range[16,64,65] and the overall charge distribution of the protein.[66,67] Figure 5C also shows that the magnitudes of both the inner- and outer-shell contributions to $\langle F_{C=O} \rangle$ are markedly larger for amide-containing solutes (DMA, NMA, and 1,3-dimethylurea). The larger inner-shell contributions for the amides arise from their propensity to form more HBs than non-amides (i.e., they have on average higher n_{HB} values, Table S16), and their individual HBs also turn out to be stronger on

https://doi.org/10.1021/acs.jpcb.2c03095
J. Phys. Chem. B 2022, 126, 5876−5886

average due to enhanced solute−solvent polarization. For example, going from acetone to 1,3-dimethylurea, the change in the total inner-shell solvent electric field (32.7 MV/cm) is partially attributed to a shift in the distribution of n_{HB}, which accounts for 16.0 MV/cm of the field difference. This estimate is based on the linear correlation relating n_{HB} to the inner-shell field contribution (Figure 5A); that is, we substituted the $\langle n_{HB}\rangle$ values of acetone (1.505) and 1,3-dimethylurea (2.234) into the fitted linear correlation for acetone ($F^{in}_{C=O} = -23.542n_{HB} + 37.321$, $R^2 = 0.991$) and then evaluated the difference between the resulting fields. The remaining 16.7 MV/cm difference in solvent-induced field on these two solutes is then attributed to the enhancement of field contributed by individual HBs. Note that this increase in individual HB's field contribution is expected to be more pronounced with fields calculated by using DFT because in QM calculations the inner-shell solvent molecules can be strongly polarized by the solute, an effect that is not captured by the fixed-charge MM calculations. In terms of the outer-shell contributions to $\langle F_{C=O}\rangle$, the particularly large values for NMA and 1,3-dimethylurea are consistent with the increased ordering of the second coordination shell as observed in their $O_w\cdots O_c$ RDFs (Figure S6).

Altogether, Figure 5 demonstrates that our solvent electric field decomposition scheme based on DFT calculations can successfully separate the field into an n_{HB}-dependent inner-shell component ($r_{O_wO_c} \leq 3.5$ Å) and an n_{HB}-independent outer-shell component ($r_{O_wO_c} > 3.5$ Å). In contrast, one could additionally invoke a commonly employed angular cutoff for HBs ($\angle H-O_w-O_c < 30°$), which combines the water molecules in the first solvation shell that do not meet the angular criterion yet have strong HB character, with the outer-shell ones (see Figure S10A for the average populations of the first solvation shell by HB and non-HB waters and Figure S10B for the distribution of $\angle H-O_w-O_c$ for each solute). However, in doing so, we find a strong dependence of the bulk (non-HB) contribution to the field on n_{HB}, which then inversely correlates with the HB component of the field (see Figure S11). This demonstrates that even geometrically distorted HBs (those with $\angle H-O_w-O_c > 30°$) that fall radially within the first solvation shell ($r_{O_wO_c} \leq 3.5$ Å) make a significant contribution to the field (Tables S17 and S18).

CONCLUSIONS

Using a combined experimental and computational approach, we have demonstrated in this work that amide carbonyl groups are subjected to substantially larger electric fields arising from polar solvent environments, which can be nearly twice as strong as those on non-amide carbonyls, such as ketones, esters, and thioesters. This gives rise to the markedly larger vibrational solvatochromic shifts of the amide-containing compounds. Our MD simulations for a wide variety of solute−solvent systems show that amide carbonyls induce more pronounced solvent organizations around them, as indicated by their more prominent first solvation peaks in the RDFs and the larger average number of HBs they form in protic solvents than non-amides, giving rise to the more substantial electric fields they experience in solution. This ability of the amide-containing solutes to induce local solvent ordering originates from the substantial $p-\pi$ conjugation between the amide sp^2-nitrogens and the carbonyl groups, which increases the polarity of the amide C=O bonds. By employing a scheme based on DFT calculations, we demonstrated that one can decompose the total solvent electric field exerted on C=O into contributions from the inner- and outer-shell solvent molecules, which show strong and little dependence on the number of HBs, respectively. Performing this decomposition for all six solutes in water reveals that the larger electric fields experienced by the amide carbonyls arise from a combination of their propensity to form more HBs, the enhanced field contribution per HB, and their larger field contributions from solvent molecules in the bulk. In contrast to previous studies that have correlated the large frequency shifts of amide carbonyls in water with the lengths of HBs they form[62,68] or the electron-donating ability of the C=O groups,[69] our results show that the magnitudes of these solvatochromic shifts are determined by the electrostatic environments and can be quantitatively mapped from a simple physical descriptor, that is, the projection of solvent electric field along the C=O bond, based on the linear vibrational Stark effect.

Our findings further substantiate the electrostatic model where solvent molecules organize themselves to stabilize solute bond dipoles[57] and suggest approaches to modulate the electrostatic environment experienced by a solute via modifying its own molecular structure. Such an understanding provides an important implication for the design of new vibrational Stark probes; that is, these probes should minimally perturb the environment so that they can be employed for *in-situ* measurements of electric fields in complex environments. Furthermore, in biological catalysis it has been suggested that preorganized electrostatic environments in the active sites of enzymes play a central role in their catalytic functionality,[16,34,70] a principle that has been used to guide the design of mutated enzymes as well as biomimetic catalysts. The multiple effects that lead to the greater electric fields experienced by amide carbonyls described in this work, on the other hand, suggest the possibility of an alternative substrate (solute)-centric approach to achieving electrostatic environments that are favorable to catalysis; that is, one can induce preorganization in the environment by introducing chemically inert but electrostatically consequential structural motifs to the substrate.[71] Our combined experimental and computational approaches employed in this work will provide a route to elucidating the physics underlying these electrostatics-inspired strategies for catalyst design.

ASSOCIATED CONTENT

Supporting Information

The Supporting Information is available free of charge at https://pubs.acs.org/doi/10.1021/acs.jpcb.2c03095.

Further details on the vibrational Stark effect; results and analysis from vibrational Stark spectroscopy; details on infrared spectral features; supplementary results on solvent organization and electric fields from MD simulations; corresponding data figures for each section; supplementary tables (PDF)

AUTHOR INFORMATION

Corresponding Authors

Thomas E. Markland − *Department of Chemistry, Stanford University, Stanford, California 94305, United States;* orcid.org/0000-0002-2747-0518; Email: tmarkland@stanford.edu

https://doi.org/10.1021/acs.jpcb.2c03095
J. Phys. Chem. B 2022, 126, 5876−5886

Steven G. Boxer − *Department of Chemistry, Stanford University, Stanford, California 94305, United States;* orcid.org/0000-0001-9167-4286; Email: sboxer@stanford.edu

Authors

Steven D. E. Fried − *Department of Chemistry, Stanford University, Stanford, California 94305, United States;* orcid.org/0000-0002-4826-2451

Chu Zheng − *Department of Chemistry, Stanford University, Stanford, California 94305, United States;* orcid.org/0000-0003-3309-208X

Yuezhi Mao − *Department of Chemistry, Stanford University, Stanford, California 94305, United States;* orcid.org/0000-0001-5362-4333

Complete contact information is available at: https://pubs.acs.org/10.1021/acs.jpcb.2c03095

Notes

The authors declare no competing financial interest.

■ ACKNOWLEDGMENTS

This work was supported in part by the National Science Foundation Grant Nos. MCB-1915727 (to S.G.B.) and CHE-2154291 (to T.E.M.) as well as the National Institutes of Health Grant R35GM118044 (to S.G.B.). S.D.E.F. is supported by the NSF Graduate Research Fellowship under Grant DGE-1656518, C.Z. is supported the Stanford Center for Molecular Analysis and Design (CMAD) Fellowship, and T.E.M. also acknowledges support from the Camille Dreyfus Teacher-Scholar Awards Program. This research also used resources of the National Energy Research Scientific Computing Center (NERSC), a U.S. Department of Energy Office of Science User Facility operated under Contract DE-AC02-05CH11231, and the Sherlock cluster operated by the Stanford Research Computing Center.

■ REFERENCES

(1) Mabesoone, M. F. J.; Palmans, A. R. A.; Meijer, E. W. Solute−Solvent Interactions in Modern Physical Organic Chemistry: Supramolecular Polymers as a Muse. *J. Am. Chem. Soc.* **2020**, *142* (47), 19781−19798.

(2) Reichardt, C.; Welton, T. *Solvents and Solvent Effects in Organic Chemistry*, 4th ed.; John Wiley & Sons: Weinheim, Germany, 2010.

(3) Davis, C. M.; Gruebele, M.; Sukenik, S. How does solvation in the cell affect protein folding and binding? *Curr. Opin. Struct. Biol.* **2018**, *48*, 23−29.

(4) Wilson, A. D.; Stetson, C. Modeling solution vapor equilibria with solvation and solute assembly. *J. Mol. Liq.* **2021**, *336*, 116272.

(5) Donon, J.; Habka, S.; Vaquero-Vara, V.; Brenner, V.; Mons, M.; Gloaguen, E. Electronic Stark Effect in Isolated Ion Pairs. *J. Phys. Chem. Lett.* **2019**, *10* (23), 7458−7462.

(6) Lin, C.-Y.; Romei, M. G.; Oltrogge, L. M.; Mathews, I. I.; Boxer, S. G. Unified Model for Photophysical and Electro-Optical Properties of Green Fluorescent Proteins. *J. Am. Chem. Soc.* **2019**, *141* (38), 15250−15265.

(7) Fried, S. D.; Boxer, S. G. Measuring Electric Fields and Noncovalent Interactions Using the Vibrational Stark Effect. *Acc. Chem. Res.* **2015**, *48* (4), 998−1006.

(8) Andrews, S. S.; Boxer, S. G. Vibrational Stark Effects of Nitriles II. Physical Origins of Stark Effects from Experiment and Perturbation Models. *J. Phys. Chem. A* **2002**, *106* (3), 469−477.

(9) Cho, M. Vibrational solvatochromism and electrochromism: Coarse-grained models and their relationships. *J. Chem. Phys.* **2009**, *130* (9), 094505.

(10) Reichardt, C. Solvatochromic Dyes as Solvent Polarity Indicators. *Chem. Rev.* **1994**, *94* (8), 2319−2358.

(11) Choi, J.-H.; Cho, M. Vibrational solvatochromism and electrochromism of infrared probe molecules containing C≡O, C≡N, C═O, or C−F vibrational chromophore. *J. Chem. Phys.* **2011**, *134* (15), 154513.

(12) Levinson, N. M.; Fried, S. D.; Boxer, S. G. Solvent-Induced Infrared Frequency Shifts in Aromatic Nitriles Are Quantitatively Described by the Vibrational Stark Effect. *J. Phys. Chem. B* **2012**, *116* (35), 10470−10476.

(13) Fried, S. D.; Wang, L.-P.; Boxer, S. G.; Ren, P.; Pande, V. S. Calculations of the Electric Fields in Liquid Solutions. *J. Phys. Chem. B* **2013**, *117* (50), 16236−16248.

(14) Fried, S. D.; Bagchi, S.; Boxer, S. G. Measuring Electrostatic Fields in Both Hydrogen-Bonding and Non-Hydrogen-Bonding Environments Using Carbonyl Vibrational Probes. *J. Am. Chem. Soc.* **2013**, *135* (30), 11181−11192.

(15) Liu, C. T.; Layfield, J. P.; Stewart, R. J.; French, J. B.; Hanoian, P.; Asbury, J. B.; Hammes-Schiffer, S.; Benkovic, S. J. Probing the Electrostatics of Active Site Microenvironments along the Catalytic Cycle for Escherichia coli Dihydrofolate Reductase. *J. Am. Chem. Soc.* **2014**, *136* (29), 10349−10360.

(16) Fried, S. D.; Bagchi, S.; Boxer, S. G. Extreme electric fields power catalysis in the active site of ketosteroid isomerase. *Science* **2014**, *346* (6216), 1510−1514.

(17) Schneider, S. H.; Boxer, S. G. Vibrational Stark Effects of Carbonyl Probes Applied to Reinterpret IR and Raman Data for Enzyme Inhibitors in Terms of Electric Fields at the Active Site. *J. Phys. Chem. B* **2016**, *120* (36), 9672−9684.

(18) Schneider, S. H.; Kozuch, J.; Boxer, S. G. The Interplay of Electrostatics and Chemical Positioning in the Evolution of Antibiotic Resistance in TEM β-Lactamases. *ACS Cent. Sci.* **2021**, *7* (12), 1996−2008.

(19) Tanford, C.; Kirkwood, J. G. Theory of protein titration curves. I. General equations for impenetrable spheres. *J. Am. Chem. Soc.* **1957**, *79* (20), 5333−5339.

(20) Lum, K.; Chandler, D.; Weeks, J. D. Hydrophobicity at Small and Large Length Scales. *J. Phys. Chem. B* **1999**, *103* (22), 4570−4577.

(21) Patel, A. J.; Varilly, P.; Jamadagni, S. N.; Acharya, H.; Garde, S.; Chandler, D. Extended surfaces modulate hydrophobic interactions of neighboring solutes. *Proc. Natl. Acad. Sci. U. S. A.* **2011**, *108* (43), 17678.

(22) Gorman, C. B.; Marder, S. R. An investigation of the interrelationships between linear and nonlinear polarizabilities and bond-length alternation in conjugated organic molecules. *Proc. Natl. Acad. Sci. U. S. A.* **1993**, *90* (23), 11297.

(23) Marder, S. R.; Perry, J. W.; Tiemann, B. G.; Gorman, C. B.; Gilmour, S.; Biddle, S. L.; Bourhill, G. Direct observation of reduced bond-length alternation in donor/acceptor polyenes. *J. Am. Chem. Soc.* **1993**, *115* (6), 2524−2526.

(24) Bublitz, G. U.; Ortiz, R.; Marder, S. R.; Boxer, S. G. Stark Spectroscopy of Donor/Acceptor Substituted Polyenes. *J. Am. Chem. Soc.* **1997**, *119* (14), 3365−3376.

(25) Onsager, L. Electric Moments of Molecules in Liquids. *J. Am. Chem. Soc.* **1936**, *58* (8), 1486−1493.

(26) Tapia, O.; Goscinski, O. Self-consistent reaction field theory of solvent effects. *Mol. Phys.* **1975**, *29* (6), 1653−1661.

(27) Marten, B.; Kim, K.; Cortis, C.; Friesner, R. A.; Murphy, R. B.; Ringnalda, M. N.; Sitkoff, D.; Honig, B. New Model for Calculation of Solvation Free Energies: Correction of Self-Consistent Reaction Field Continuum Dielectric Theory for Short-Range Hydrogen-Bonding Effects. *J. Phys. Chem.* **1996**, *100* (28), 11775−11788.

(28) Tomasi, J.; Mennucci, B.; Cammi, R. Quantum Mechanical Continuum Solvation Models. *Chem. Rev.* **2005**, *105* (8), 2999−3094.

(29) Marenich, A. V.; Cramer, C. J.; Truhlar, D. G. Universal Solvation Model Based on Solute Electron Density and on a Continuum Model of the Solvent Defined by the Bulk Dielectric

Constant and Atomic Surface Tensions. *J. Phys. Chem. B* **2009**, *113* (18), 6378−6396.
(30) Mennucci, B. Polarizable continuum model. *Comput. Mol. Sci.* **2012**, *2* (3), 386−404.
(31) Hille, C.; Ringe, S.; Deimel, M.; Kunkel, C.; Acree, W. E.; Reuter, K.; Oberhofer, H. Generalized molecular solvation in non-aqueous solutions by a single parameter implicit solvation scheme. *J. Chem. Phys.* **2019**, *150* (4), 041710.
(32) Herbert, J. M. Dielectric continuum methods for quantum chemistry. *Comput. Mol. Sci.* **2021**, *11* (4), e1519.
(33) Gersch, M.; Kreuzer, J.; Sieber, S. A. Electrophilic natural products and their biological targets. *Nat. Prod. Rep.* **2012**, *29* (6), 659.
(34) Warshel, A.; Russell, S. T. Calculations of electrostatic interactions in biological systems and in solutions. *Q. Rev. Biophys.* **1984**, *17* (3), 283−422.
(35) Wang, X.; Li, Y.; He, X.; Chen, S.; Zhang, J. Z. H. Effect of Strong Electric Field on the Conformational Integrity of Insulin. *J. Phys. Chem. A* **2014**, *118* (39), 8942−8952.
(36) Phillips, M. A.; Fletterick, R.; Rutter, W. J. Arginine 127 stabilizes the transition state in carboxypeptidase. *J. Biol. Chem.* **1990**, *265* (33), 20692−20698.
(37) Nicolas, A.; Egmond, M.; Verrips, C. T.; De Vlieg, J.; Longhi, S.; Cambillau, C.; Martinez, C. Contribution of Cutinase Serine 42 Side Chain to the Stabilization of the Oxyanion Transition State. *Biochemistry* **1996**, *35* (2), 398−410.
(38) Schmeing, T. M.; Huang, K. S.; Kitchen, D. E.; Strobel, S. A.; Steitz, T. A. Structural Insights into the Roles of Water and the 2′ Hydroxyl of the P Site tRNA in the Peptidyl Transferase Reaction. *Mol. Cell* **2005**, *20* (3), 437−448.
(39) Wallin, G.; Åqvist, J. The transition state for peptide bond formation reveals the ribosome as a water trap. *Proc. Natl. Acad. Sci. U. S. A.* **2010**, *107* (5), 1888−1893.
(40) Andrews, S. S.; Boxer, S. G. A liquid nitrogen immersion cryostat for optical measurements. *Rev. Sci. Instrum.* **2000**, *71* (9), 3567−3569.
(41) Bublitz, G. U.; Boxer, S. G. Stark Spectroscopy: Applications in Chemistry, Biology, and Materials Science. *Annu. Rev. Phys. Chem.* **1997**, *48* (1), 213−242.
(42) Andrews, S. S.; Boxer, S. G. Vibrational Stark Effects of Nitriles I. Methods and Experimental Results. *J. Phys. Chem. A* **2000**, *104* (51), 11853−11863.
(43) Davari, N.; Daub, C. D.; Åstrand, P.-O.; Unge, M. Local Field Factors and Dielectric Properties of Liquid Benzene. *J. Phys. Chem. B* **2015**, *119* (35), 11839−11845.
(44) Frisch, M. J.; Trucks, G. W.; Schlegel, H. B.; Scuseria, G. E.; Robb, M. A.; Cheeseman, J. R.; Scalmani, G.; Barone, V.; Petersson, G. A.; Nakatsuji, H.; et al. *Gaussian 16, Revision A.03*; Gaussian, Inc.: Wallingford, CT, 2016.
(45) Case, D. A.; Belfon, K.; Ben-Shalom, I. Y.; Brozell, S. R.; Cerutti, D. S.; T.E. Cheatham, I.; Cruzeiro, V. W. D.; Darden, T. A.; Duke, R. E.; Giambasu, G.; et al. *AMBER 2020*; University of California: San Francisco, 2020.
(46) Krishnan, R.; Binkley, J. S.; Seeger, R.; Pople, J. A. Self-consistent molecular orbital methods. XX. A basis set for correlated wave functions. *J. Chem. Phys.* **1980**, *72* (1), 650−654.
(47) Stephens, P. J.; Devlin, F. J.; Chabalowski, C. F.; Frisch, M. J. Ab Initio Calculation of Vibrational Absorption and Circular Dichroism Spectra Using Density Functional Force Fields. *J. Chem. Phys.* **1994**, *98* (45), 11623−11627.
(48) Wang, J.; Wolf, R. M.; Caldwell, J. W.; Kollman, P. A.; Case, D. A. Development and testing of a general amber force field. *J. Comput. Chem.* **2004**, *25* (9), 1157−1174.
(49) Jakalian, A.; Jack, D. B.; Bayly, C. I. Fast, efficient generation of high-quality atomic charges. AM1-BCC model: II. Parameterization and validation. *J. Comput. Chem.* **2002**, *23* (16), 1623−1641.
(50) Caleman, C.; van Maaren, P. J.; Hong, M.; Hub, J. S.; Costa, L. T.; van der Spoel, D. Force Field Benchmark of Organic Liquids: Density, Enthalpy of Vaporization, Heat Capacities, Surface Tension, Isothermal Compressibility, Volumetric Expansion Coefficient, and Dielectric Constant. *J. Chem. Theory Comput.* **2012**, *8* (1), 61−74.
(51) Jorgensen, W. L.; Chandrasekhar, J.; Madura, J. D.; Impey, R. W.; Klein, M. L. Comparison of simple potential functions for simulating liquid water. *J. Chem. Phys.* **1983**, *79* (2), 926−935.
(52) Abraham, M. J.; van der Spoel, D.; Lindahl, E.; Hess, B.; the GROMACS development team *GROMACS User Manual version 2018*; 2018; www.gromacs.org.
(53) Abraham, M. J.; Murtola, T.; Schulz, R.; Páll, S.; Smith, J. C.; Hess, B.; Lindahl, E. GROMACS: High performance molecular simulations through multi-level parallelism from laptops to supercomputers. *SoftwareX* **2015**, *1−2*, 19−25.
(54) Bussi, G.; Donadio, D.; Parrinello, M. Canonical sampling through velocity rescaling. *J. Chem. Phys.* **2007**, *126* (1), 014101.
(55) Parrinello, M.; Rahman, A. Polymorphic transitions in single crystals: A new molecular dynamics method. *J. Appl. Phys.* **1981**, *52* (12), 7182−7190.
(56) Epifanovsky, E.; Gilbert, A. T. B.; Feng, X.; Lee, J.; Mao, Y.; Mardirossian, N.; Pokhilko, P.; White, A. F.; Coons, M. P.; Dempwolff, A. L.; et al. Software for the frontiers of quantum chemistry: An overview of developments in the Q-Chem 5 package. *J. Chem. Phys.* **2021**, *155* (8), 084801.
(57) Zheng, C.; Mao, Y.; Kozuch, J.; Atsango, A. O.; Ji, Z.; Markland, T. E.; Boxer, S. G. A two-directional vibrational probe reveals different electric field orientations in solution and an enzyme active site. *Nat. Chem.* **2022**, DOI: 10.1038/s41557-022-00937-w.
(58) Claudino, D.; Mayhall, N. J. Automatic Partition of Orbital Spaces Based on Singular Value Decomposition in the Context of Embedding Theories. *J. Chem. Theory Comput.* **2019**, *15* (2), 1053−1064.
(59) Luzar, A.; Chandler, D. Hydrogen-bond kinetics in liquid water. *Nature* **1996**, *379* (6560), 55−57.
(60) Böttcher, C. J. F.; van Belle, O. C.; Bordewijk, P.; Rip, A. *Theory of Electric Polarization*, 2nd ed.; Elsevier Pub. Co.: Amsterdam, The Netherlands, 1973; Vol. *1*.
(61) Schneider, S. H.; Kratochvil, H. T.; Zanni, M. T.; Boxer, S. G. Solvent-Independent Anharmonicity for Carbonyl Oscillators. *J. Phys. Chem. B* **2017**, *121* (10), 2331−2338.
(62) Hamm, P.; Lim, M.; Hochstrasser, R. M. Structure of the Amide I Band of Peptides Measured by Femtosecond Nonlinear-Infrared Spectroscopy. *J. Phys. Chem. B* **1998**, *102* (31), 6123−6138.
(63) Bagchi, S.; Fried, S. D.; Boxer, S. G. A Solvatochromic Model Calibrates Nitriles' Vibrational Frequencies to Electrostatic Fields. *J. Am. Chem. Soc.* **2012**, *134* (25), 10373−10376.
(64) Wang, L.; Fried, S. D.; Markland, T. E. Proton Network Flexibility Enables Robustness and Large Electric Fields in the Ketosteroid Isomerase Active Site. *J. Phys. Chem. B* **2017**, *121* (42), 9807−9815.
(65) Welborn, V. V.; Head-Gordon, T. Fluctuations of Electric Fields in the Active Site of the Enzyme Ketosteroid Isomerase. *J. Am. Chem. Soc.* **2019**, *141* (32), 12487−12492.
(66) Wade, R. C.; Gabdoulline, R. R.; Lüdemann, S. K.; Lounnas, V. Electrostatic steering and ionic tethering in enzyme−ligand binding: Insights from simulations. *Proc. Natl. Acad. Sci. U. S. A.* **1998**, *95* (11), 5942.
(67) Gunasekaran, K.; Pentony, M.; Shen, M.; Garrett, L.; Forte, C.; Woodward, A.; Ng, S. B.; Born, T.; Retter, M.; Manchulenko, K.; et al. Enhancing Antibody Fc Heterodimer Formation through Electrostatic Steering Effects: Applications to Bispecific Molecules and Monovalent IgG. *J. Biol. Chem.* **2010**, *285* (25), 19637−19646.
(68) Hamm, P.; Lim, M.; DeGrado, W. F.; Hochstrasser, R. M. Stimulated Photon Echoes from Amide I Vibrations. *J. Phys. Chem. A* **1999**, *103* (49), 10049−10053.
(69) Harnagea, E. I.; Jagodzinski, P. W. Infrared spectra of cyclic and non-cyclic ureas in solution: structures and interactions. *Vib. Spectrosc.* **1996**, *10* (2), 169−175.
(70) Warshel, A.; Sharma, P. K.; Kato, M.; Xiang, Y.; Liu, H.; Olsson, M. H. M. Electrostatic Basis for Enzyme Catalysis. *Chem. Rev.* **2006**, *106* (8), 3210−3235.

(71) Walker, T. W.; Chew, A. K.; Li, H.; Demir, B.; Zhang, Z. C.; Huber, G. W.; Van Lehn, R. C.; Dumesic, J. A. Universal kinetic solvent effects in acid-catalyzed reactions of biomass-derived oxygenates. *Energy Environ. Sci.* **2018**, *11* (3), 617−628.

https://doi.org/10.1021/acs.jpcb.2c03095
J. Phys. Chem. B 2022, 126, 5876−5886

Supplementary Information

Solvent Organization and Electrostatics Tuned by Solute Electronic Structure: Amide versus Non-Amide Carbonyls

Steven D.E. Fried,[1] Chu Zheng,[1] Yuezhi Mao,[1] Thomas E. Markland,[1]* and Steven G. Boxer[1]*

[1]Department of Chemistry, Stanford University, Stanford, California 94305, USA

*Corresponding Authors. Emails: tmarkland@stanford.edu; sboxer@stanford.edu

Contents

I. Vibrational Stark Effect Supplement

The Vibrational Stark Tuning Rate

The change in transition energy $\Delta\bar{\nu}$ between two levels (e.g., electronic, vibrational) in a molecule is perturbed by the molecule's electrostatic environment according to the Stark effect. If $\vec{F}$ is the applied field directed on the molecule (either externally or by the molecule's solvent environment), then the perturbation of $\Delta\bar{\nu}$ to second order is described by

$$\Delta\bar{\nu} = -\Delta\vec{\mu}\cdot\vec{F} - \tfrac{1}{2}\vec{F}\cdot\underline{\Delta\alpha}\cdot\vec{F}\,, \tag{1.1}$$

where $\Delta\vec{\mu}$ is the change in dipole moment or the Stark tuning rate and $\underline{\Delta\alpha}$ the change in polarizability between the two levels.[1] The two terms describing this perturbation are known as the linear and quadratic Stark effects, respectively. In the case of a vibrational transition, an increase in dipole moment typically accompanies a transition from ground to first excited state due to the anharmonicity of the molecular oscillator. In the simple case of a vibrational mode localized to a particular bond, as the equilibrium bond length increases between the two states, so too does charge separation between the two atoms and thus $\Delta\vec{\mu}$ is positive. For bonds such as the carbonyls investigated herein and nitriles, the first-order term is large and the second-order term is typically negligible over most relevant ranges in electric field.[2]

There are multiple ways to assess a molecule's vibrational Stark tuning rate $|\Delta\vec{\mu}|$. The most direct is to measure the ground- and excited-state dipole moments and take the difference.[3] Such methods can be performed in the gas phase, but since high accuracy of the raw measurements are necessary for a reasonably accurate difference dipole, this is only applicable to a limited selection of small molecules.[4] Alternatively, one can consider that the chief reason for the difference dipole $|\Delta\vec{\mu}|$ lies in anharmonicity, causing the equilibrium bond distance to increase by Δd between the ground and first excited states:

$$\Delta\mu = q\Delta d = 3\left|\vec{m}\right|\sqrt{\chi_{\mathrm{e}}}\,, \tag{1.2}$$

where q is the charge separation, $|\vec{m}|$ is the magnitude of the transition dipole moment of the oscillator, and χ_{e} is the anharmonicity constant as used in the Morse oscillator.[5] The anharmonicity constant χ_{e} can be determined spectroscopically using overtone absorption[6] or two-dimensional infrared spectroscopy,[7] where the parameter is defined for two vibrational modes $\bar{\nu}_{0\to1}$ and $\bar{\nu}_{1\to2}$ as $\chi_{\mathrm{e}} = (\bar{\nu}_{0\to1} - \bar{\nu}_{1\to2})/\bar{\nu}_{\mathrm{e}}$, with $\bar{\nu}_{\mathrm{e}}$ denoting the frequency of the unperturbed harmonic oscillator. Note that this method also suffers limitations: for instance, the challenge of accurate determination of $|\vec{m}|$ for the vibrational probe in vacuum, as well as the assumption that the anharmonicity constant χ_{e} remains approximately constant in diverse solvents. The latter assumption breaks down in cases of substantial bond polarization, where the solvent environment perturbs a solute's electronic structure such that bond properties, including length, force constant, charge separation, and anharmonicity all change accordingly. However, previous results from 2D IR spectroscopy have indicated that χ_{e} for simple carbonyls like acetophenone is largely constant across diverse solvent environments, supporting the notion that the Stark tuning rate is an intrinsic property of carbonyl-based vibrational probes rather than a consequence of solvent-perturbed electronic structure changing the bond anharmonicity.[7]

The two methods that we use for the determination of $|\Delta\vec{\mu}|$ are vibrational Stark spectroscopy (VSS), where the effect of an applied external electric field on the transition is measured, and vibrational solvatochromism paired with molecular dynamics simulations. Both solvatochromism and VSS rely on the vibrational Stark effect itself to observe frequency shifts in the vibrational spectrum and link them to the electric field environment that a vibrational probe

experiences. In the case of solvatochromism, this field is produced by the variable solvent environment, whereas in VSS an applied external field is responsible for the frequency shift. Solvatochromism is experimentally simple, and the range of polar and nonpolar solvents typically available for most molecules mean that a wide range of fields can be applied. However, solvatochromism is insufficient by itself as a means of determining the Stark tuning rate—the frequency shift data must be combined with data of the ensemble-averaged electric field on the probe, which can be calculated using forces from a molecular dynamics (MD) trajectory.[8] In this case, the slope of the fitted linear correlation between experimentally observed frequency and ensemble-averaged electric field for each solvent gives an apparent $|\Delta\vec{\mu}|$. Because the determination of $|\Delta\vec{\mu}|$ by vibrational solvatochromism and molecular dynamics is inherently a hybrid method and potentially suffers from issues associated with the force field and precise method of field calculation, it is helpful to also use a purely empirical approach. Vibrational Stark spectroscopy in an applied external electric field is a purely experimental technique, but this method introduces its own complexities,[1] making a combination of methods the most applicable approach to characterize $|\Delta\vec{\mu}|$.[4]

Vibrational Stark Spectroscopy and Analysis

A key aspect of the Stark effect is the vector representation of the field and dipole interactions (e.g., equation 1.1). A Stark shift will be magnified when $\Delta\vec{\mu}$ is either parallel or antiparallel to the applied electric field $\vec{F}$, the former orientation causing a red-shift of the transition frequency due to increased stabilization of the excited-state oscillator dipole, and the latter orientation causing a blue shift. In solvatochromism, solvent organization about a solute effectively explores an ensemble of various configurations, though the weighted average will favor a parallel relationship between solvent field and molecular dipole, producing a red shift that increases with greater solvent polarity.[4] In vibrational Stark spectroscopy, an external electric field is applied to a sample consisting of a vibrational probe immobilized in a frozen glass. This should preserve the isotropic distribution of solvent and solute molecules with respect to the laboratory frame as in solvatochromism, however, local interactions during glass formation may complicate this (see below). Because the molecules are isotropically oriented relative to the applied field, some will shift red, others will shift blue, and most will have very little shift at all—leading to an overall band broadening effect. Consequently, the difference spectrum between the field-on and field-off spectrum results in a lineshape that is the second-derivative of the absorption band due to band broadening, so long as the field perturbation is smaller than the inhomogeneous linewidth (essentially always the case) in accordance with the linear Stark effect.[1] A change in polarizability, on the other hand, will perturb energy levels in the same direction independently of the direction of $\Delta\vec{\mu}$, resulting in a uniform shift of the infrared absorption peak and a first-derivative of absorption lineshape in the field-on minus field-off difference spectrum.[1]

It follows that we can extract the relevant parameters $|\Delta\vec{\mu}|$ and $\underline{\Delta\alpha}$ through fitting of the zeroth, first, and second derivatives of an absorbance spectrum to the field-on minus field-off Stark difference spectrum. For the case of isotropic, immobilized solutes, the change in absorption upon application of an external electric field is given by a linear combination of these derivative components.[1, 9-10]

$$\Delta A(\bar{\nu}) = F^2 \left\{ A_\chi A(\bar{\nu}) + \frac{B_\chi}{15hc}\bar{\nu}\frac{d}{d\bar{\nu}}\left(\frac{A(\bar{\nu})}{\bar{\nu}}\right) + \frac{C_\chi}{30h^2c^2}\bar{\nu}\frac{d^2}{d\bar{\nu}^2}\left(\frac{A(\bar{\nu})}{\bar{\nu}}\right)\right\}, \qquad (1.3)$$

where the parameters A_χ, B_χ, and C_χ, are defined as follows:

$$A_\chi = \frac{1}{30|\vec{m}|^2}\sum_{ij}\left[10A_{ij}^2 + \left(3\cos^2\chi - 1\right)\left(3A_{ii}A_{jj} + A_{ij}^2\right)\right] + \frac{1}{15|\vec{m}|^2}\sum_{ij}\left[10m_iB_{ijj} + \left(3\cos^2\chi - 1\right)(4m_iB_{ijj})\right],$$

$$B_\chi = \frac{5}{2}\mathrm{Tr}\left(\underline{\Delta\alpha}\right) + \left(3\cos^2\chi - 1\right)\left(\frac{3}{2}\underline{\Delta\alpha}_m - \frac{1}{2}\mathrm{Tr}\left(\underline{\Delta\alpha}\right)\right) + \frac{1}{|\vec{m}|^2}\sum_{ij}\left[10m_iA_{ij}\Delta\mu_j + \left(3\cos^2\chi - 1\right)(3m_iA_{jj}\Delta\mu_i + m_iA_{ij}\Delta\mu_j)\right],$$

and $$C_\chi = |\Delta\vec{\mu}|^2 \cdot \left[5 + \left(3\cos^2\chi - 1\right)\left(3\cos^2\zeta_\mathrm{A} - 1\right)\right].$$

Here, $\underline{A}$ and $\underline{\underline{B}}$ are tensors describing the transition polarizability and transition hyperpolarizability, respectively, and they reflect the influence of the electric field on the transition moment $\vec{m}\left(\vec{F}\right) = \vec{m} + \underline{A}\cdot\vec{F} + \vec{F}\cdot\underline{\underline{B}}\cdot\vec{F}$.[1] Moreover, χ is the experimental angle between the applied field and polarization of the incident light, ζ_A is the angle between the difference dipole $\Delta\vec{\mu}$ and the transition moment $\vec{m}$, and $\underline{\Delta\alpha}_m$ is the component of the polarizability change projected along the direction of the transition moment (that is, $\underline{\Delta\alpha}_m = \vec{m}\underline{\Delta\alpha}\vec{m}/|\vec{m}|^2$).[1] Indices *i* and *j* denote individual components of the vectors and tensors and run over the molecular coordinates *x, y,* and *z*.

The analysis of the vibrational Stark spectra described in the main text used the above equations, with several key simplifying assumptions. The determination of $|\Delta\vec{\mu}|$ is entirely from the third coefficient C_χ, where the polarization of the incident light relative to the applied field is 90°,[1] and where the angle ζ_A between the difference dipole $\Delta\vec{\mu}$ and the transition moment $\vec{m}$ is assumed to be zero. Taking ζ_A to be zero is generally a good assumption. Firstly, for symmetric molecules such as acetone or dimethylurea, both $\Delta\vec{\mu}$ and $\vec{m}$ should be parallel to the carbonyl, making the angle between the vectors exactly zero. For asymmetric molecules including the esters and amides investigated herein, the $\Delta\vec{\mu}$ and $\vec{m}$ vectors may deviate slightly from the direction of the carbonyl, but if both $\Delta\vec{\mu}$ and $\vec{m}$ skew from the carbonyl bond together, then ζ_A will still be close to zero. However, let us consider a potential case where the two vectors do not skew together from the direction of the bond vector. The deviation of $\vec{m}$ for a carbonyl from the direction of the bond dipole will not be large; for instance, in glycine dipeptide the orientation of $\vec{m}$ differs from the carbonyl bond vector by 10°.[11] Even if we assume that the angle ζ_A between $\Delta\vec{\mu}$ and $\vec{m}$ is also 10°, this will still translate to a small (~1.5%) relative change in the final calculated value of $|\Delta\vec{\mu}|$ using equation 1.3, which is on the order of the experimental error itself.[12] Hence for small perturbations of ζ_A depending on the molecular electronic structure, the assumption that ζ_A = 0 is reasonable for carbonyls. Note that it is also possible to determine ζ_A experimentally by varying the angle χ of the incident light relative to the applied field—helpful in cases of doubt, such as for other types of vibrational probes contained in even more asymmetric systems.

The primary complication in using vibrational Stark spectroscopy for the calibration of vibrational probes lies in the correction for deviations in the local field from the external applied field. Although the external applied field can be known accurately, there is typically a difference in the local field experienced by a chromophore or vibrational probe in solution, resulting from changes in dielectric constant between the solvent and the solute cavity. The field $\vec{F}$ experienced by the molecule is related to the external field $\vec{F}_{ext}$ according to $\vec{F} = \underline{f}\cdot\vec{F}_{ext}$, where $\underline{f}$ is the local field correction tensor, which can usually be approximated as a scaler f.[1] A number of models have been proposed to estimate the value of this correction term using the dielectric constants of

the solvent and solute, plus the size and shape of the solute cavity.[13] While to this day no reliable experimental approach has been described that can consistently yield the value of f in diverse solvent-solute systems, its value is currently thought to be close to 2, based on comparison of VSS Stark tuning rates with those given by other complementary methods.[4] Using this approach, the Stark tuning rate determined by fitting the absorption spectrum second derivative to the Stark difference spectrum is treated as $|\Delta\vec{\mu}_{C=O}|f$, which is compared to the $|\Delta\vec{\mu}_{C=O}|$ method derived from other methods above, particularly solvatochromism with molecular dynamics simulations. A subtle and confounding issue for frozen glasses (or polymer matrices) is the possibility that the organization of the solvent molecules around the solute may be affected by the local bond dipole of the solute and the solvent dipoles,[14] as seen in the fluid phase simulations reported in the current work. We are not aware of a reliable way to evaluate the local solvent organization in frozen glasses and how this may affect $|f|$.

VSS data for two molecules, acetone and 1,3-dimethylurea, were combined with previous data collected for ethyl thioacetate, ethyl acetate, *N*-methylacetamide, and dimethylacetamide.[12] The most consistently successful glass-forming solvent was 2-methyltetrahydrofuran. Fig. S1 shows Stark spectra of a mixture of acetone and 1,3-dimethylurea. Analysis using Eqn. 1.3 gives $|\Delta\vec{\mu}_{C=O}|f$ = 0.74 cm^{-1}/(MV/cm) for acetone, significantly lower than that of the other molecules. This qualitatively matches its lower Stark tuning rate from solvatochromism, 0.31 cm^{-1}/(MV/cm). Analysis of the 1,3-dimethylurea Stark spectrum is complicated by the appearance of another overlapping vibrational mode at ~1580 cm^{-1}. While this mode was also present in room-temperature vibrational solvatochromism, it appears a special case in the low-temperature absorbance spectra where the carbonyl stretch mode is sufficiently blue-shifted to overlap with this second mode. Note that out of the two modes observed in the IR, the higher-frequency one corresponds to the carbonyl stretch (symmetry *A*'). The heterogeneous

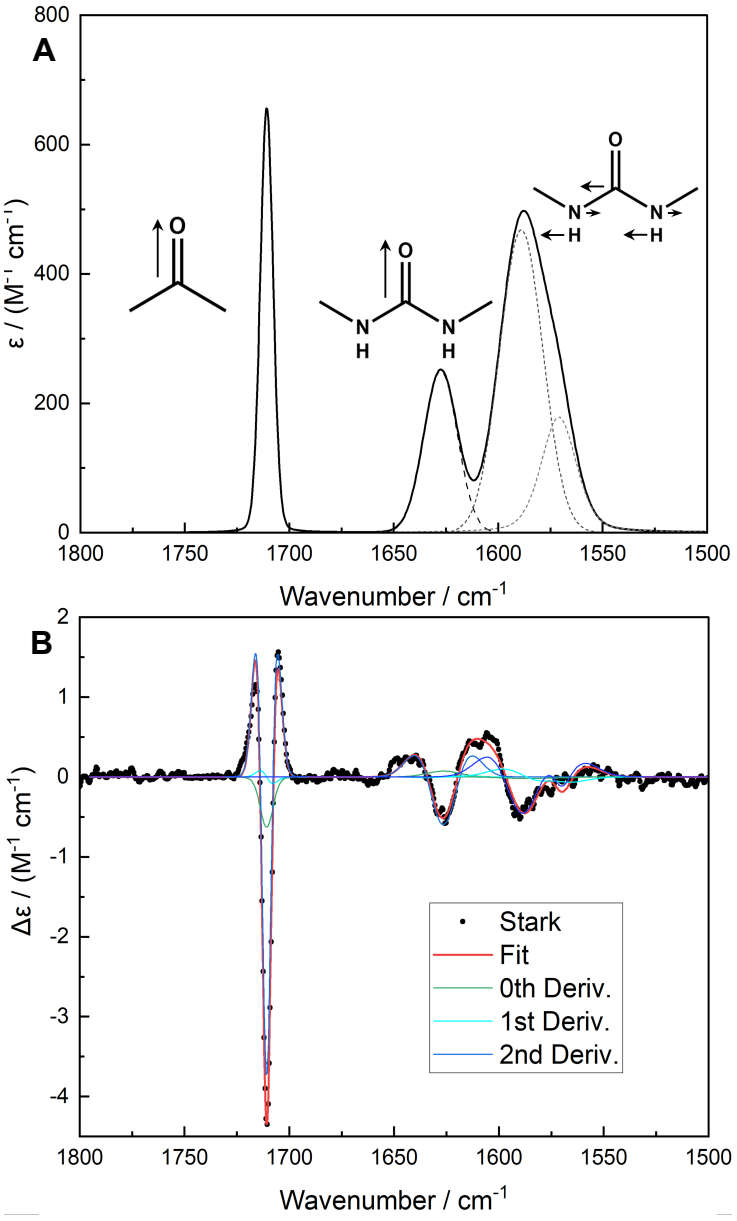

FIGURE S1. Vibrational Stark spectra of acetone and 1,3-dimethylurea. (A) 77K absorption spectra of 51 mM acetone and 50 mM 1,3-dimethylurea together in 2-methyl-tetrahydrofuran. The spectrum of 1,3-dimethylurea is complicated by two overlapping vibrational modes (see text). (B) Stark spectra fit to 0th, 1st, and 2nd-derivatives of the absorption Voigt profiles (data scaled to 1 MV/cm, obtained at 0.7 MV/cm applied field) for acetone and 1,3-dimethylurea.

lower-frequency one corresponding to a global bending mode of symmetry *A*", where the carbonyl carbon and amide hydrogens together move antiparallel to the motion of the amide nitrogen, coupled to bending of the methyl C-H bonds. Hence, we fit the Stark spectrum to the derivatives of two separate peaks (one composite) and report the Stark tuning rate $|\Delta\vec{\mu}_{C=O}|f$ of the higher-frequency C=O stretch to be 1.24 MV/cm, in the same range as the amides and esters.

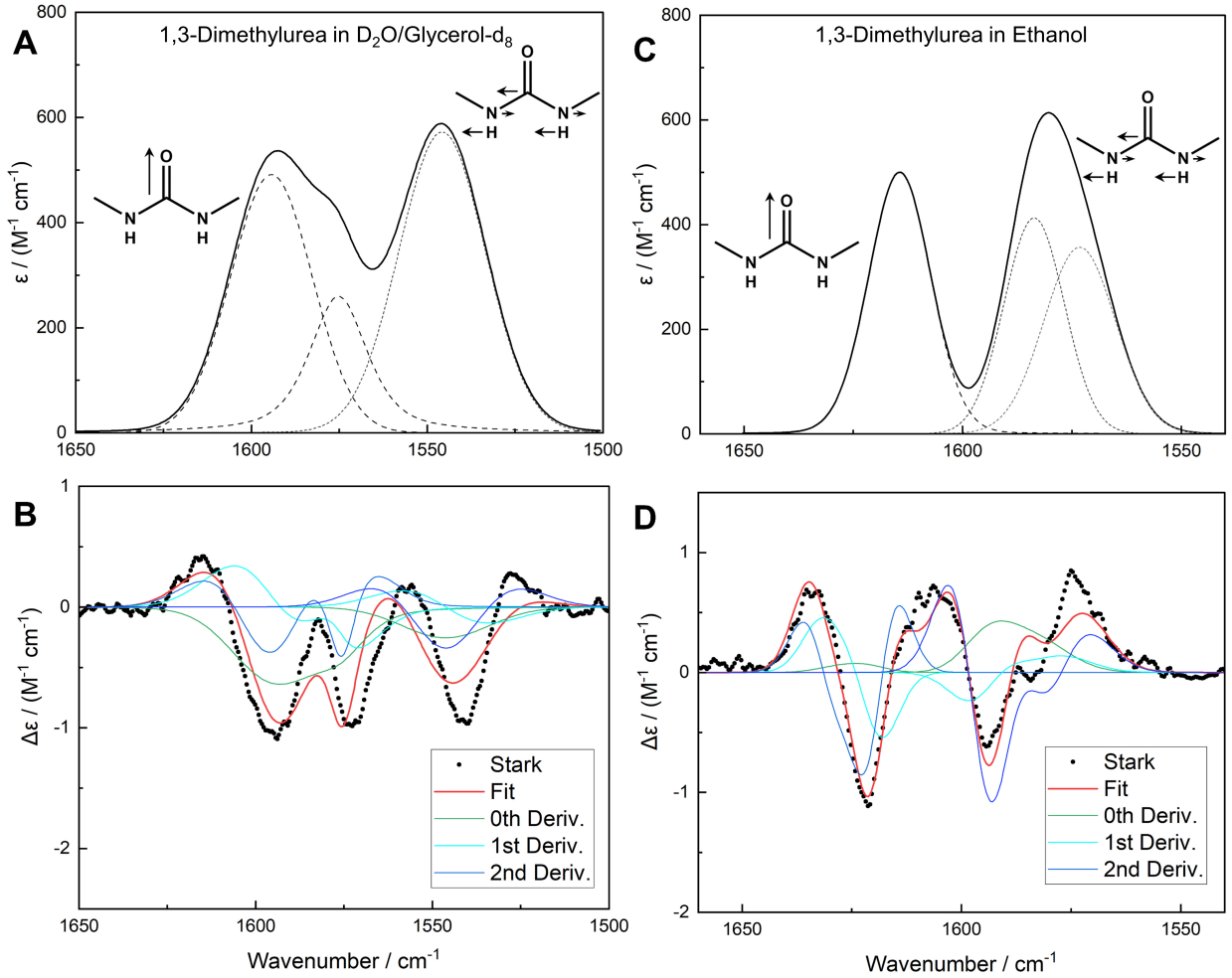

FIGURE S2. Vibrational Stark spectra of 1,3-dimethylurea in different solvents. (A) 77K absorption spectra of 57 mM 1,3-dimethylurea in 1:1 mixture of D_2O:glycerol-d_8. The spectrum of 1,3-dimethylurea is complicated by two overlapping vibrational modes (see text). (B) Stark spectra of 1,3-dimethylurea in D_2O:glycerol-d_8 fitted to 0^{th}, 1^{st}, and 2^{nd}-derivatives of the absorption Voigt profiles (obtained at 1 MV/cm applied field). (C) 77K absorption spectra of 50 mM 1,3-dimethylurea in ethanol. (D) Stark spectra of 1,3-dimethylurea in ethanol fitted to 0^{th}, 1^{st}, and 2^{nd}-derivatives of the absorption Voigt profiles (obtained at 1 MV/cm applied field).

In addition to 2-methyltetrahydrofuran, 1,3-dimethylurea was also subjected to Stark spectroscopy in ethanol as well as a 1:1 mixture of D_2O:glycerol-d_8 (Figure S2). This was done in part to determine whether the two overlapping vibrational modes could be better resolved. In D_2O-glycerol 1:1, the resolution between the two peaks was worse than in 2-methyltetrahydrofuan, leading to a worse fit by zeroth, first, and second derivatives of the absorption spectrum. Due to the lower second-derivative contribution to the fit, the $|\Delta\vec{\mu}_{C=O}|f$ value determined is also lower, 1.1 cm^{-1} /(MV/cm). The high contributions of the 0^{th} and 1^{st}-order derivatives is a sign that these results are not as reliable as those in 2-methyltetrahydrofuran. In ethanol, the separation between the two peaks is slightly better, but the fit to the derivatives is also quite poor due to high

contributions of the zeroth and first derivatives of the absorption spectrum. The poor quality of the fit is manifested in an abnormally small Stark tuning rate for the carbonyl, $|\Delta\vec{\mu}_{\mathrm{C=O}}|f$ = 0.9 MV/cm, which is slightly smaller than the value determined by solvatochromism and not a good indication of the true $|\Delta\vec{\mu}_{\mathrm{C=O}}|$. As a possible explanation, note that for some solutes such as nitriles, hydrogen bonding may influence the polarizability of a molecule and reduce the applicability of the linear Stark effect,[15] and it could be that a related effect is observed here in the hydrogen-bonding environment of ethanol. Because 2-methyltetrahydrofuran yields the best fitting results and was also the solvent glass of choice for comparing the results with Schneider et al.,[12] we report these values in the main text.

The results of the VSS measurements for each compound are summarized in Table 1 of the main text. Generally, the carbonyl Stark tuning rates obtained from VSS, $|\Delta\vec{\mu}_{\mathrm{C=O}}|f$, appear in the same general range as the previously considered molecules ethyl thioacetate, ethyl acetate, dimethylacetamide, and *N*-methylacetamide.[12] By contrast, the IR frequency changes in solvatochromism can vary quite widely for the various carbonyl-containing molecules. We attribute the wide variability in $\Delta\bar{\nu}_{\mathrm{C=O}}$ despite small variability in $|\Delta\vec{\mu}_{\mathrm{C=O}}|f$ to the differences in solvent-induced electric field $\vec{F}_{\mathrm{C=O}}$ between the various molecules. The additional molecules considered here, acetone and 1,3-dimethylurea, have $|\Delta\vec{\mu}_{\mathrm{C=O}}|f$ values that reflect, in part, their respective Stark tuning rates from solvatochromism. Comparison of the two sets of values, $|\Delta\vec{\mu}_{\mathrm{C=O}}|f$ from VSS and $|\Delta\vec{\mu}_{\mathrm{C=O}}|$ from solvatochromism, means that the value of the local field factor f may be estimated as the scaling factors between them (Table 1 last column).

The estimation of the local field factor f in this manner yields a relatively small value of *f* for 1,3-dimethylurea (~1.2), whereas f grows progressively larger for molecules such as esters and amides (~1.7–1.9), acetone (~2.4) and even greater yet for ethylthioacetate (~2.7). This apparent variation in f as a result of the solute identity is striking, and may be a reflection of solute polarizability. For instance, we note that the ordering of *f* qualitatively matches the ordering of the polarizabilities of the atoms directly adjacent to the carbonyl: oxygen and nitrogen have the lowest atomic polarizabilities α ($0.88 \cdot 10^{-24}$ cm^3 and $1.1 \cdot 10^{-24}$ cm^3, respecitvely), followed by carbon ($1.67 \cdot 10^{-24}$ cm^3) and then sulfur ($2.87 \cdot 10^{-24}$ cm^3) whose significantly greater polarizability arises from being a period lower.[16] More polarizable groups directly next to the carbonyl will enhance the field experienced by the carbonyl and thus increase the value of *f*. Beyond solute polarizabiliy, we also suspect that solute size and shape play a role in the local field correction,[13] while the electronic structure of the solute influences solvent organization about itself as we describe in the main text. Hence, there can be multiple levels of simultaneous action, where the intrinsic properties of the solute (e.g., polarizability of groups near the carbonyl) as well as its effects on solvent organization together influence how an externally applied field is locally experienced along the carbonyl bond in a solute. Practically speaking, however, we see that variations in Stark tuning rate observed in either VSS or solvatochromism experiments do not adequately account for the drastic frequency shifts of amides and dimethylurea in polar solvents, confirming that a strong electrostatic interaction is occurring in these solute-solvent systems.

Vibrational Solvatochromism

Vibrational Stark spectroscopy and vibrational solvatochromism paired with molecular dynamics simulations for electric field calculations are used in this work and others[8, 12, 17] as complementary approaches towards obtaining the true Stark tuning rate $|\Delta\vec{\mu}|$ of a vibrational probe. Both methods have their advantages and limitations: while VSS is a purely experimental method, the results are complicated by a local field factor that is currently difficult to assign with certainty. Solvatochromism plus molecular dynamics does not suffer this limitation since the

observed Stark tuning rate does not include a local field factor; however, it is inherently a hybrid approach and only as accurate as the computational method used to determine the fields (which shall be visited in the next section). The vibrational solvatochromism experiment itself is simple to perform, requiring only the collection of FTIR spectra for the vibrational probe in a range of solvents. The analysis too is generally straightforward, though occasionally some challenges arise in the identification of the correct vibrational mode of interest from a spectrum. For instance, acetone's spectrum includes a peak near 1744 cm^{-1} that in the least polar solvents (e.g., hexanes, dibutyl ether) appears as a shoulder peak. However, the identity of this peak appears to be a combination band consisting of a CC stretch together with a CO in-plane bending mode of symmetry designations ν_{17} and ν_{19}, respectively, an observation that has been reported previously in the literature.[18] This assignment is supported by the observation that this second shoulder peak does not appear concentration dependent (Figure S3). Because this peak is irrelevant to the solvatochromic shift of the carbonyl stretch caused by electric fields projected along C=O, compound peaks such as these were fit with two Voigt functions, with only the peak corresponding to the main (C=O stretch) peak used in the field-frequency correlations for determination of $|\Delta\vec{\mu}_{C=O}|$.

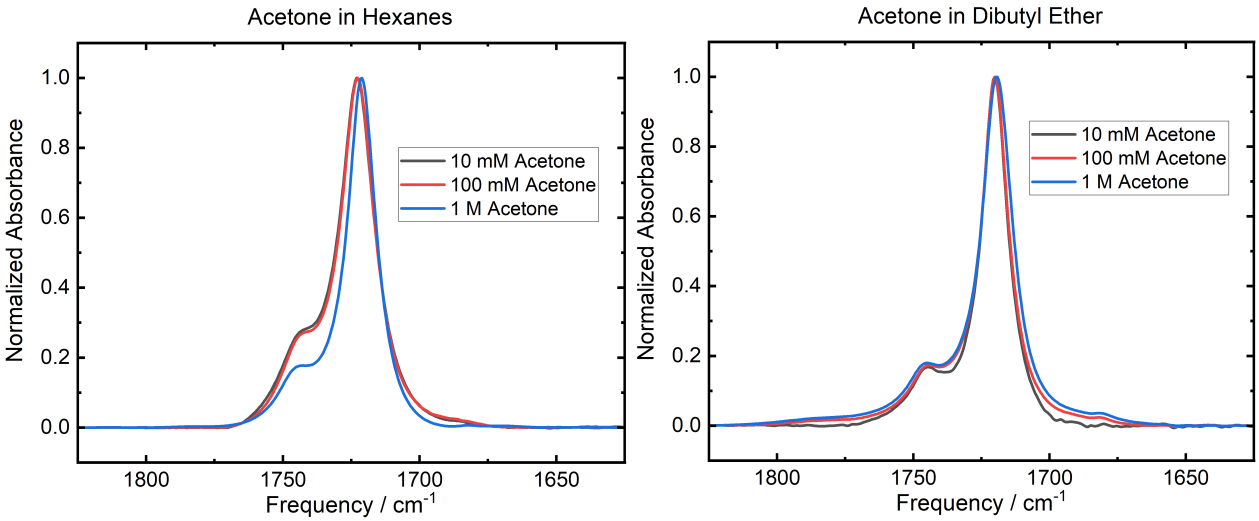

FIGURE S3. Concentration dependence of acetone in nonpolar solvents does not reveal a clear concentration dependence of the blue-shifted shoulder peak, which is more likely a combination band.

In another example, we also observe a shoulder feature for *N*-methylacetamide dissolved in the least polar solvents (Figure S4). In this case, however, the feature does appear to be concentration dependent: as we increase concentration, the red-shifted shoulder peak grows, indicating the existence of dimers which have been experimentally[19] and theoretically[20] characterized in the literature. Dimers are red-shifted due to increased electrostatics parallel to the carbonyl dipole in the dimer versus the hexanes-solvated monomer. Similarly to as with acetone, we fit the 10 mM spectrum with two Voigt functions and disregard the dimer shoulder.

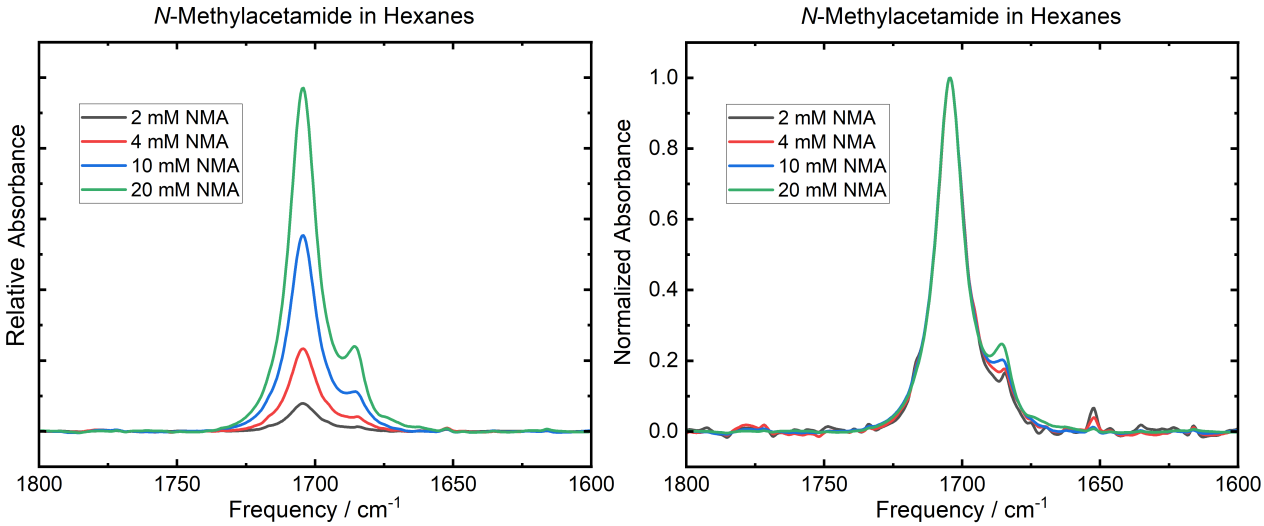

FIGURE S4. Concentration dependence of acetone in nonpolar solvents does not reveal a clear concentration dependence of the blue-shifted shoulder peak, which is more likely a combination band.

In several other spectra, including for dimethylurea in more polar solvents, as well as occasionally for acetone in THF, NMA in dibutyl ether, and several of the spectra from Schneider et al.[12] we notice that one peak is not sufficient to fit the main carbonyl peak left after accounting for known dimer or combination bands. These asymmetric spectra likely result from heterogeneity in the solvation environment, as we note that they are more common to observe for solutes that form more hydrogen bonds such as those containing an amide motif. Usually, the spectral asymmetries are not prominent or distinct enough in frequency to be clearly recognizable as a separate mode. For spectra such as these, we undertook a more conservative analysis approach by fitting the asymmetric spectrum with two Voigt populations. We then took a weighted average of the peak positions according to the peak intensities, therefore finding the ensemble average carbonyl frequency in the potentially heterogeneous solvation environment. The parameters used in the spectral fitting analysis for both symmetric and asymmetric peaks are shown in Tables S1-S6, where the average peak positions are used in the field-frequency correlation plots of the main text (main text Figure 3).

One final point to note concerns our use of field-frequency calibrations from solvatochromism to obtain fields in more complex environments, including proteins.[2] Solvatochromism provides such calibrations irrespective of how solvent-solute mutual interactions come in (e.g., whether through hydrogen bonding, dipole, or dispersion interactions). For the majority of carbonyls thus investigated,[12] this analysis works and gives strongly linear dependencies of the frequency shift on the calculated electric field in both protic and aprotic solvents—a result both predicted by electronic structure calculations[21] and shown experimentally by infrared spectroscopy.[2] By contrast, nitriles deviate from this trend due to unique electronic structure effects resulting from hydrogen bonding between solvent and the N atom.[15, 22-23] It is thus critical to select a vibrational probe for which a linear field-frequency relationship holds, as such a probe can then be used to quantify electrostatics of diverse types of interactions in complex environments such as protic protein interiors[2] and solvation spheres about conformationally flexible and charged solutes.[24]

As an indication of the applicability of the solvatochromic approach to handling both protic and aprotic solvent conditions, we also conduct linear fits of the field-frequency plots from main text Figure 3 where the water points are omitted (Figure S5). In fact, removing the water points typically only changes the calibration fitting parameters marginally and inconsistently. When comparing each of the slopes including water molecules to those excluding water molecules, we find that the changes are usually small compared to the fitting error (Table S8). For instance, none of the differences in slope are statistically significant at the 95% confidence level, and only the slope change of dimethylacetamide is significant at the 90% confidence level (*p*-value = 0.059, all other *p*-values > 0.17, calculated using a t-test to compare slopes of regression lines).[25] Moreover, when the slopes do change between including or excluding the water points, they do not do so in the same direction each time: for *N*-methylacetamide and 1,3-dimethylurea, the slopes marginally decrease upon excluding water, but for the other solutes, the slopes marginally increase. Indeed, this indicates that inclusion of water does not have a systematic effect on the Stark tuning rates, nor does it have a consistent effect on the quality of fit indicated by the correlation coefficient (Table S8). These results seem to suggest that covalency involved in water hydrogen bonding, or potential charge transfer effects, have no significant or systematic effect on the calibrated Stark tuning rates, but rather the inclusion of water as an additional point will extend the calibration range of the Stark probes to increase accuracy of $\Delta\mu$ determination.

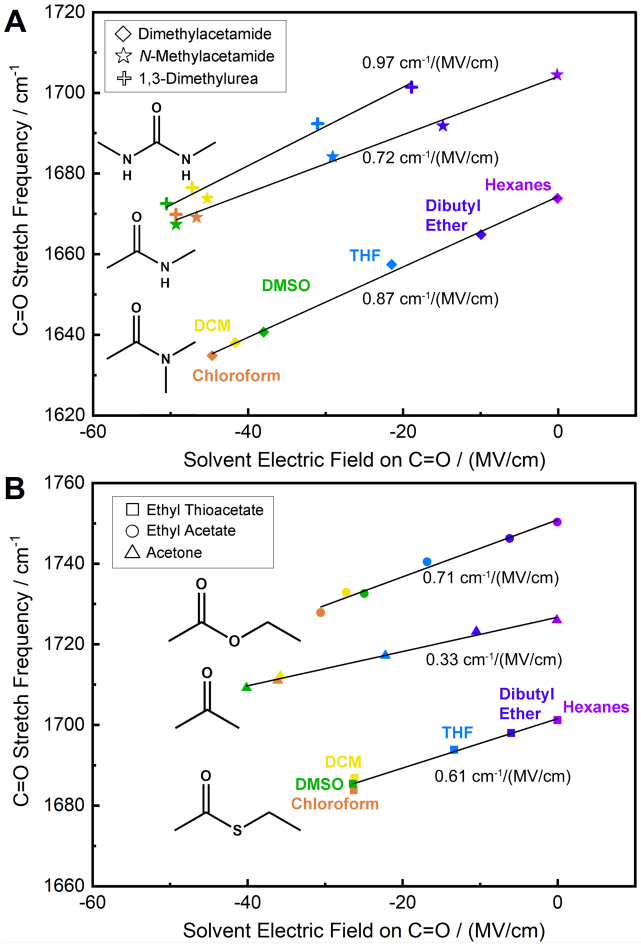

FIGURE S5. Field-frequency correlation plots for (A) smaller-field carbonyl-containing molecules (ester, thioester, ketone) and (B) larger-field amide and dimethylurea molecules, in an analogy to main text Figure 3 but excluding water points. Slopes of the linear correlations (apparent Stark tuning rates $|\Delta\vec{\mu}_{C=O}|$) are provided next to each line.

II. Solvation Molecular Dynamics Simulations Supplement

Solvent organization about solute carbonyls was characterized in this work by a variety of different metrics using 1-ns molecular dynamics trajectories of the solutes in a wide range of solvents. For characterization of the radial distribution function (RDF) of solvent organization around the carbonyl oxygens, trajectories were used with coordinates saved every 2 fs, while for other measurements snapshots separated by 200-fs intervals were sufficient. Here we show RDFs for each of the solvents used in the simulations set—water, methanol, chloroform, dichloromethane, dimethyl sulfoxide, dibutyl ether, tetrahydrofuran, and hexanes (Figure S6). Each RDF is defined for the position of the hydrogen bond donor atom (or solvent carbon atom for aprotic solvents) relative to the solute carbonyl oxygen. We see that each of the protic solvents water, methanol, and chloroform displays a very well-defined first solvation sphere about the carbonyl, with smaller radii ($r_{max} \approx 2.7$ Å, defined by distance to the first peak maximum in $g(r)$) in the cases of the canonical protic solvents water and methanol, and a greater radius ($r_{max} \approx 3.3$ Å) in the case of chloroform, which forms weak HB interactions with carbonyls.[26] For all six carbonyl-containing solutes evaluated, the progressively less polar solvents demonstrate first solvation shells of lower amplitudes with greater distances to the probability maxima.

From the RDFs, we see that the primary distinction in solvation structure around amide versus non-amide carbonyls resides in the population of the first solvation shell related to the integral under the first peak, which is greater for amides and dimethylurea and smaller for the other molecules. Hence, the average number of HBs, rather than HB distance, appears to play a bigger role in mediating the differences in solvent electrostatic environments across varying solutes. Note that a well-defined first-solvation shell is still observed for dichloromethane, suggesting the presence of strong dipole-dipole interactions or even weak hydrogen bonds. For increasingly hydrophobic solvents (tetrahydrofuran, dibutyl ether and hexanes), solvent ordering about the carbonyl decreases, which thus more closely resembles the distribution of solvent in the bulk

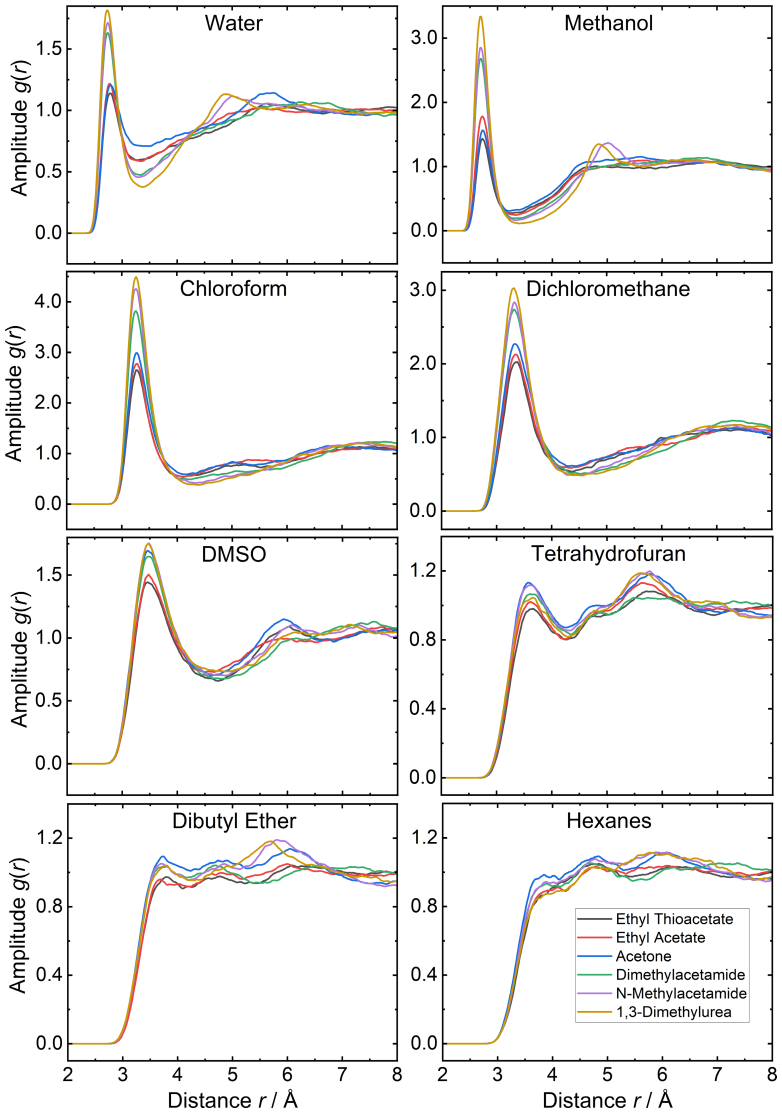

FIGURE S6. Radial distribution functions $g(r)$ for six carbonyl-containing solutes in solvents of a wide range of polarities. The calculated RDFs were smoothed with a 0.1-Å rolling average for clarity.

phase. We also see less distinction in the amplitude of the RDFs between the different solutes for the least polar solvents, indicating the correspondingly diminished relevance of electrostatics-mediated solvent organization about the carbonyls.

Together, the RDFs reveal a scenario involving significant organization of the most polar solvents (e.g., water, methanol, chloroform) about the solute carbonyls compared to the least polar ones (e.g., dibutyl ether, tetrahydrofuran, hexanes) as expected. Although these trends are seen for each of the six solutes investigated, they are magnified in the case of the amide and dimethylurea molecules, for which the more pronounced first solvation shells in their RDFs indicate increased probability of close interactions. Many of the molecules in these first solvation shells could be considered hydrogen bonds according to the geometric criteria described in the main text. Indeed, enumerating the average number of hydrogen-bonded solvent molecules for each solute molecule reveals a strong dependence on solute electronic structure, where both amides and dimethylurea have the greatest number of these interactions. Furthermore, the average number of hydrogen bonds appears strongly correlated with the electric field measured on each carbonyl-containing molecule (main text Figure 4). The correlation between hydrogen bond number and the strength of solvent-induced electric field on the carbonyl across different solutes is not limited only to the ensemble-averaged hydrogen bond number. We also see that within individual trajectories, a greater number of hydrogen bonds correlates with stronger electric fields. Examples of these correlations are demonstrated in Figure S7 for the cases of ethyl thioacetate and 1,3-dimethylurea in water, using the electric fields and hydrogen bond numbers per trajectory frame calculated using the classical MD approach.

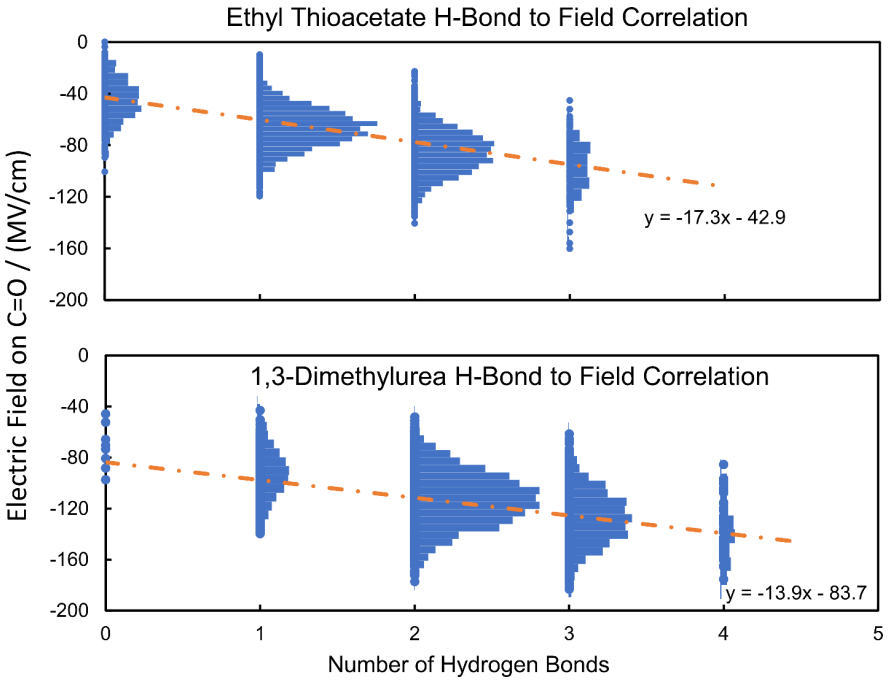

FIGURE S7. Distribution of electric field strength along the carbonyls of ethyl thioacetate (upper) and 1,3-dimethylurea (lower) in aqueous solutions within each group of trajectory frames as characterized based on the number of hydrogen bonds in each MD frame.

A distribution of field magnitudes was obtained for each possible number of hydrogen bonds, as indicated by the superimposed histograms. A linear regression through the classically determined fields reveals a slope that changes only minimally despite the diversity in molecule types and the magnitudes of the ensemble-averaged solvent electric fields. Indeed, the two greatest changes between the ethyl thioacetate (lowest field) and 1,3-dimethylurea (strongest

field) results are the shift in the statistical weight of each HB-number group (resulting in changes to the ensemble-averaged number of hydrogen bonds) and the change in *y*-intercepts (representing the average field in the group of frames with zero hydrogen bonds). This field, designated by the *y*-intercept (-42.9 MV/cm for ethyl thioacetate and -83.7 MV/cm for 1,3-dimethylurea), arises from both inner-shell non-hydrogen–bonding waters as well as outer-shell bulk solvent. Similar results are confirmed by DFT analysis (main text Figure 5), where the overall field on C=O increases in a similar way for each solvent as the number of hydrogen bonds increases, while the number of hydrogen bonds varies with the solute, and the non-hydrogen–bonding contribution is typically shifted by a constant value depending on the solute.

Using this same approach for each of the six different solutes in water, we similarly determine linear correlations between the MD-calculated electric field strengths along the carbonyl bonds and the corresponding number of hydrogen bonds formed in those respective trajectory frames. The best-fit lines to these data are shown in in Figure S8, plotted as solid lines. Also plotted are the ensemble averages for both field and hydrogen bond number for each solute in water, represented as individual, single points. We note that both the hydrogen bond number, on the *x*-axis, and the non-hydrogen–bonding field contribution (related to the *y*-intercept) change as the solute identity changes. This gives rise to a strongly correlated *universal* trend (patterned line) between average hydrogen bond number and average electric field, for six diverse carbonyl-containing solvents. These observed trends linking average hydrogen bond number to average field are plotted for methanol and chloroform solvents, in addition to water, in Figure 4 of the main text.

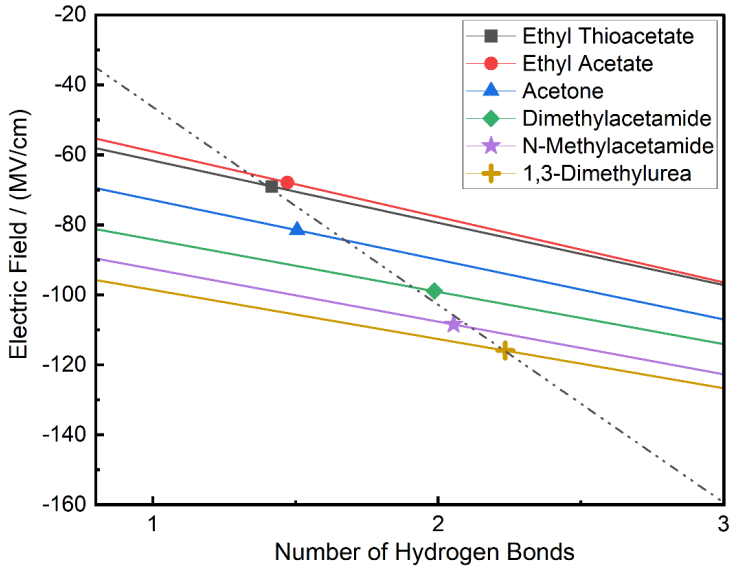

FIGURE S8. Linear regressions (solid) are plotted to describe the approximate relationship between the electric field projection on C=O and the number of HBs for each individual frame within an MD-trajectory. The linear relationships are shown for each of six solute molecules in water. Another correlation (patterned line) across different solutes results from the ensemble-averaged (single points) number of HBs and solvent electric field on C=O in a given MD trajectory.

While the solvent-induced electric field on the carbonyl generally increases with more hydrogen bonds, we also begin to see reasons why this correlation should not be perfectly linear even when the fields are calculated using the classical force field. Looking at the distribution of hydrogen-bond distances between the solute carbonyl and the solvent water molecules (Figure S9), we see that the mean hydrogen-bond length increases with additional hydrogen bonds, i.e., the hydrogen bonds are weakened when more are present, likely as the solvent molecules experience more steric congestion as more of them interact simultaneously with the carbonyl.

More broadly, these results likely reflect a complicated tradeoff between solvent-solvent interactions and solvent-solute interactions, governed by the local (molecular) concentration of either species in a small volume element at a time,[27] as well as solvent size and structure.[28] The decrease in hydrogen bond length observed here translates to a slight decrease in the hydrogen-bond–induced electric field contribution. This gives rise to the slight curvature in the inner-shell water contribution to the electric field plotted in main text Figure 5B. Intriguingly, the mean hydrogen-bond length only changes slightly between the weakest-field solute, ethyl acetate, and the strongest-field solute, 1,3-dimethylurea, for a given number of hydrogen bonds (Table S5).

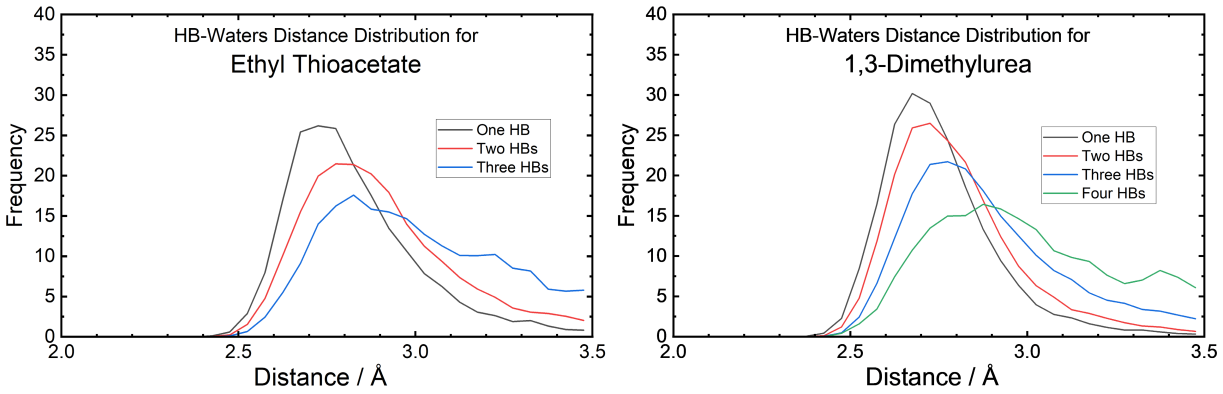

FIGURE S9. Distributions of donor-to-acceptor distance *r*(C=O···O-H) for all hydrogen bonds involving the carbonyls of ethyl thioacetate or 1,3-dimethylurea in aqueous solutions.

So far, we have considered the hydrogen-bonding (HB) solvent within the first solvation shell of the carbonyl. However, other non-hydrogen-bonding (non-HB) solvent molecules may also be present within the first solvation shell, making it important to determine the average number of either kind of solvent molecule (HB or non-HB). These values for each of the six solute molecules investigated are shown in Figure S10A in the case of water. Note that a solute's ability to form hydrogen bonds increases as charge separation along the dipole occurs due to the more pronounced p-π conjugation in amides and dimethylurea. Correspondingly, the number of non-HB solvent molecules within the first shell typically decreases with increasing HB numbers in the case of water.

In the decomposition of the first solvation shell into HB and non-HB solvent molecules shown in Fig. S10A, it is important to recall that the distinction between the two is defined geometrically. In the case of water hydrogen bonding to solute carbonyls, this implies an $O_w \cdots O_c$ distance within 3.5 Å and the H-O_w-O_c angle below 30°. Within those constraints, it is helpful to understand the distribution of HBs in terms of solvent molecule orientation with respect to the solute carbonyl (Figure S10B), particularly as an indication of how many solvent molecules are close to being identified as HB-forming but slightly fall outside of the 30° angular cutoff. Two maxima describe the most probable orientations—approximately 10° and 105°—indicating hydrogen bonding between one of the two hydrogens on water and the solute carbonyl. While non-hydrogen–bonding waters may also reside in the first solvation shell (defined out to 3.5 Å), they become less probable for amides and 1,3-dimethylurea since their increased C=O bond dipoles attract more first-shell water molecules to form HBs. Because the angular distribution shows no hard cutoff in reality for interactions at 30°, but rather a continuum, the result warrants some caution in using the geometric HB criterion for separating the solvent-induced electric field into HB- and non-HB contributions due to the near-HB waters (i.e., those in the first solvation shell but have $\angle$H-O_w-O_c > 30°, as we shall see next).

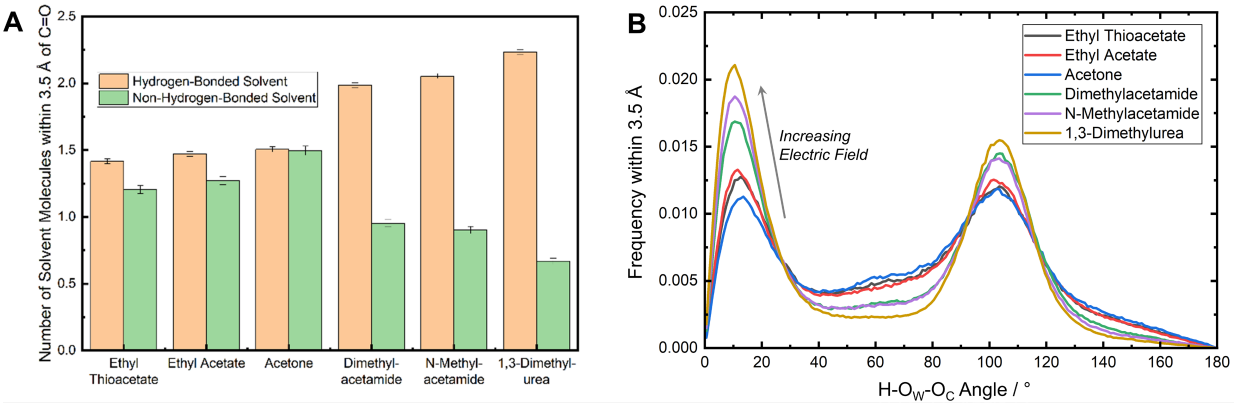

FIGURE S10. (A) Average number of hydrogen bonds formed with the solute carbonyl oxygen, together with the average number of non-hydrogen-bonding solvent molecules within the first solvation shell of the carbonyl ($r_{O_wO_c}$ < 3.5 Å) for six carbonyl-containing molecules in water. (B) Distribution of water molecule orientation angle (between water hydrogen H, water oxygen O_w, and solute carbonyl oxygen O_c) within the first solvation shell of carbonyl-containing solutes.

As a counterpart of main text Figure 5, we can perform a similar analysis to decompose the total solvent-induced electric field into HB and non-HB (rather than inner- and outer-shell) contributions (Figure S8). By combining the water molecules in the first solvation shell that do not meet the angular criterion ($\angle$H-O_w-O_c < 30°) with the outer-shell ones, we find a strongly nonlinear correlation between n_{HB} and the HB solvent contribution to $\langle F_{C=O} \rangle$ (Figure S11A), which indicates decreased individual HB strengths as the first shell becomes increasingly crowded and is in line with the larger HB distances at higher n_{HB} values (Figure S9A). This trend continues up to four HBs to the carbonyl of certain solutes as defined geometrically, though these are weaker interactions. Concurrently, we observe a strong dependence of the bulk (non-HB) contribution to the field on n_{HB}, which then inversely correlates with the HB component of the field (Figure S11B). In frames where few HBs are identified according to the geometric criteria, it is possible for several near-HB solvent molecules to be in close proximity to the carbonyl, increasing the field. Yet as HB number increases, fewer of these near-HB solvent molecules appear relevant, and the non-HB field contribution approaches an asymptotic value described by the nearly constant outer-shell contribution to the field as depicted in main text Figure 5B.

Evaluation of the ensemble-averaged contributions to the electric field along carbonyls from both HB and non-HB solvent, similar to main text Figure 5C, likewise reveals that both direct and indirect interactions play substantial roles in constituting the overall field. As shown in Figure S11C and Table S17, HB waters consistently contribute to 55-72% of the overall field, while non-HB waters contribute to 23-36%. In other words, while the field is dominated by HB effects, the non-HB effects are consequential as well. Additionally, like the inner- and outer-shell contributions, both HB and non-HB field contributions increase roughly proportionally in response to the structural modification of the solute that induces greater resonance along the carbonyl and consequently its larger bond dipole, as in the case of amides.

The simulation results altogether indicate that the solvent structure about the carbonyls of amide and dimethylurea solutes is better defined than for the carbonyls that do not exhibit appreciable *p*-π conjugation. These results are consistent with the experimental results showing stronger frequency shifts for these solutes due to solvent electrostatic environment, and whose stronger solvent-induced fields are calculated using both molecular dynamics (MD) forcefields as well as DFT methods. According to our hypothesis, these stronger fields are a consequence of a greater dipole moment along the carbonyl in amides and dimethylurea, induced by the resonance effect inherent in these molecules' electronic structure. Note that it is difficult to assign exact partial charges and bond dipole moments within a solvated molecule experimentally or theoretically—while various population analysis schemes exist to predict partial charges, these methods and the properties that they describe vary widely. We can, however, discern qualitative trends by comparing the calculated gas phase carbonyl bond dipole moments and molecular dipole moments to one another (Tables S2, S3), which generally increase for more conjugated structures such as amides/dimethylurea. The strongest correlation with field is observed in the case of the AM1-BCC charges used in the MD simulation, in agreement with intuition (main text Figure 4B). Hence, the simulation parameterizations themselves indicate the origin of the simulated electrostatic behavior of carbonyls in solution, an effect which is in good agreement with experimental results and suggests a broader trend whereby solute structure tunes solvent organization and thus the electrostatic environment.

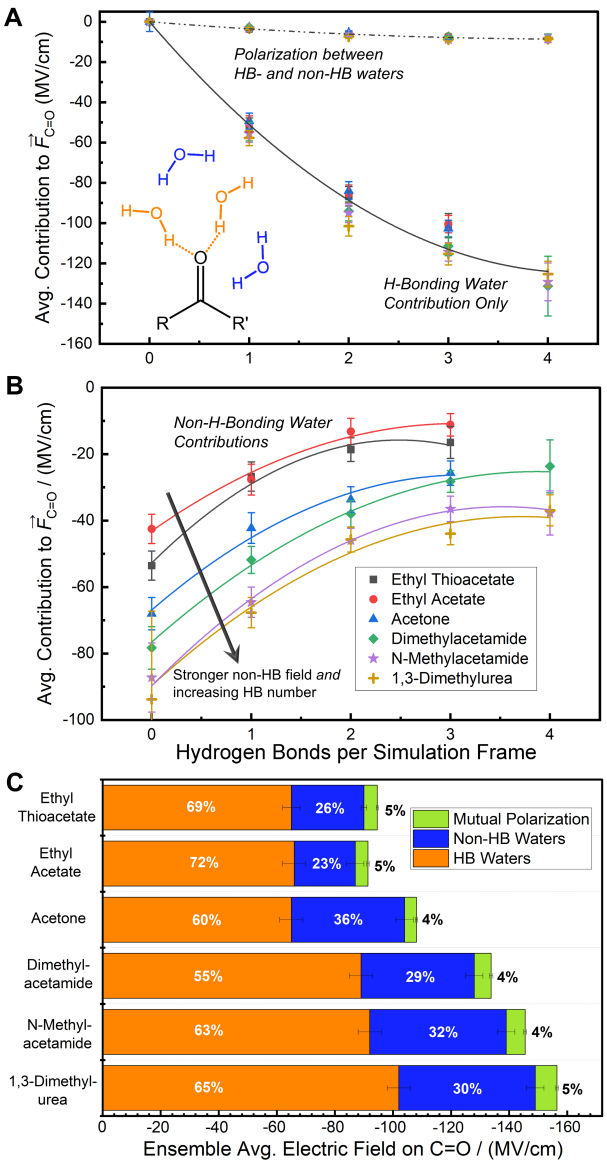

FIGURE S11. Separation of contributions to the overall electric field on carbonyls ($F_{C=O}$) for six solute molecules based on DFT calculations. (A) Electric field contributions arising from waters that form HBs with the carbonyl group (solid line) and the component of the overall field describing the polarization between the HB and non-HB waters (patterned line), both of which show similar magnitudes for different solutes (B) Field contributions from non-HB solvent water molecules, which are of larger magnitudes for amide-containing solutes. (C) Ensemble average electric field for each of the six carbonyl-containing solutes, with the absolute strengths and percentage weights of the HB, non-HB, and mutual polarization components depicted.

III. Supplemental Data Tables

TABLE S1 Ethyl thioacetate peak fitting parameters, using raw spectral data of Schneider et al.[12]

Solvent	Peak 1 Position / cm^{-1}	Peak 1 Intensity	Peak 1 Width / cm^{-1}	Peak 2 Position / cm^{-1}	Peak 2 Intensity	Peak 2 Width / cm^{-1}	Avg. Peak Position / cm^{-1}
Hexanes	1701.2	0.092	10.4				1701.2
Dibutyl Ether	1698.0	0.095	11.6				1698.0
THF	1693.9	0.089	13.3				1693.9
DMSO	1685.4	0.071	18.1				1685.4
DCM	1686.8	0.099	19.3				1686.8
Chloroform	1683.8	0.063	24.8				1683.8
Water	1663.2	0.033	35.4				1663.2

TABLE S2 Ethyl acetate peak fitting parameters, using raw spectral data of Schneider et al.[12]

Solvent	Peak 1 Position / cm^{-1}	Peak 1 Intensity	Peak 1 Width / cm^{-1}	Peak 2 Position / cm^{-1}	Peak 2 Intensity	Peak 2 Width / cm^{-1}	Avg. Peak Position / cm^{-1}
Hexanes	1750.3	0.085	9.9				1750.3
Dibutyl Ether	1746.3	0.103	10.6				1746.3
THF	1741.6	0.128	11.1	1731.4	0.015	5.6	1740.5
DMSO	1732.6	0.076	14.0				1732.6
DCM	1732.9	0.126	18.6				1732.9
Chloroform	1731.6	0.060	18.8	1718.3	0.023	27.1	1727.9
Water	1702.0	0.037	22.5	1722.7	0.020	31.2	1709.2

TABLE S3 Acetone peak fitting parameters. Note that the CC stretch + CO in-plane bending combination mode near 1750 cm^{-1} is omitted in the fitting of the carbonyl stretching peak.

Solvent	Peak 1 Position / cm^{-1}	Peak 1 Intensity	Peak 1 Width / cm^{-1}	Peak 2 Position / cm^{-1}	Peak 2 Intensity	Peak 2 Width / cm^{-1}	Avg. Peak Position / cm^{-1}
Hexanes	1722.6	0.015	15.2				1722.6
Dibutyl Ether	1719.7	0.020	11.2				1719.7
THF	1716.0	0.023	10.9	1726.4	0.003	6.4	1716.0
DMSO	1709.2	0.032	11.0				1709.2
DCM	1712.2	0.045	10.9				1712.2
Chloroform	1711.0	0.040	12.5				1711.0
Water	1697.5	0.035	15.3				1697.5

TABLE S4 Dimethylacetamide peak fitting parameters, using raw spectral data of Schneider et al.[12]

Solvent	Peak 1 Position / cm^{-1}	Peak 1 Intensity	Peak 1 Width / cm^{-1}	Peak 2 Position / cm^{-1}	Peak 2 Intensity	Peak 2 Width / cm^{-1}	Avg. Peak Position / cm^{-1}
Hexanes	1673.8	0.151	10.1				1673.9
Dibutyl Ether	1669.0	0.083	10.7	1654.5	0.033	37.1	1664.9
THF	1661.4	0.051	13.7	1651.2	0.032	33.4	1657.5
DMSO	1640.7	0.077	22.9				1640.7
DCM	1638.1	0.117	31.3				1638.1
Chloroform	1634.9	0.087	26.5				1634.9
Water	1607.8	0.111	19.7				1607.8

TABLE S5 *N*-methylacetamide peak fitting parameters. Note that the peak near 1685 cm^{-1} for NMA dimers in hexanes and dibutyl ether is omitted in the fitting of the carbonyl stretching peak.

Solvent	Peak 1 Position / cm^{-1}	Peak 1 Intensity	Peak 1 Width / cm^{-1}	Peak 2 Position / cm^{-1}	Peak 2 Intensity	Peak 2 Width / cm^{-1}	Avg. Peak Position / cm^{-1}
Hexanes	1704.5	0.005	12.1				1704.5
Dibutyl Ether	1690.0	0.013	8.1	1696.5	0.005	16.2	1691.8
THF	1684.1	0.043	9.4				1684.1
DMSO	1667.4	0.074	16.6				1667.4
DCM	1673.8	0.055	18.6				1673.8
Chloroform	1669.1	0.073	23.9				1669.1
Water	1623.2	0.041	24.3				1623.2

TABLE S6 1,3-Dimethylurea peak fitting parameters.

Solvent	Peak 1 Position / cm^{-1}	Peak 1 Intensity	Peak 1 Width / cm^{-1}	Peak 2 Position / cm^{-1}	Peak 2 Intensity	Peak 2 Width / cm^{-1}	Avg. Peak Position / cm^{-1}
Dibutyl Ether	1701.4	0.005	13.4				1701.4
THF	1692.3	0.021	15.8	1679.0	0.009	40.1	1688.4
DMSO	1672.5	0.022	30.7				1672.5
DCM	1683.9	0.017	16.1	1661.6	0.010	30.4	1676.5
Chloroform	1676.8	0.018	21.2	1659.4	0.012	31.0	1669.9
Water	1604.1	0.019	40.5				1604.1

TABLE S7 Calculated electric fields along the carbonyl bond using the classical MD approach for six carbonyl-containing solutes in a variety of solvents.

Solvent Electric Fields / (MV/cm)								
Solute	Water	Methanol	Chloroform	DCM	DMSO	THF	Dibutyl Ether	Hexanes
Ethyl Thioacetate	-69.04	-53.41	-26.33	-26.24	-26.43	-13.37	-6.02	-0.04
Ethyl Acetate	-67.92	-55.50	-30.58	-27.30	-24.96	-16.86	-6.22	-0.06
Acetone	-81.54	-70.55	-36.12	-35.77	-40.15	-22.23	-10.51	-0.12
Dimethylacetamide	-98.89	-85.35	-44.65	-41.65	-38.02	-21.49	-9.95	-0.11
N-Methylacetamide	-108.46	-96.56	-46.64	-45.29	-49.30	-29.10	-14.88	-0.14
1,3-Dimethylurea	-115.92	-105.50	-49.31	-47.22	-50.54	-31.04	-18.93	0.00

TABLE S8 Comparison of slopes (Stark tuning rates), coefficient of determination R^2, and p-values for the significance of the slopes relative to one another, when water is included or excluded as a solvent in the solvatochromic field-frequency correlation.

Solute	Slope incl. water	Slope excl. water	R^2 incl. water	R^2 excl. water	p-value for slope comparison
Ethyl Thioacetate	0.554	0.612	0.992	0.982	0.275
Ethyl Acetate	0.614	0.707	0.986	0.983	0.180
Acetone	0.315	0.325	0.991	0.976	0.715
Dimethylacetamide	0.675	0.873	0.968	0.996	0.059
N-Methylacetamide	0.745	0.721	0.996	0.988	0.590
1,3-Dimethylurea	1.018	0.974	0.997	0.978	0.578

TABLE S9 Standard deviations of the calculated electric fields along the carbonyl bond using the classical MD approach for six carbonyl-containing solutes in a variety of solvents.

Solvent Electric Field Standard Deviations / (MV/cm)								
Solute	Water	Methanol	Chloroform	DCM	DMSO	THF	Dibutyl Ether	Hexanes
Ethyl Thioacetate	21.4	24.5	12.8	12.2	11.7	8.1	5.1	0.8
Ethyl Acetate	22.6	24.0	14.1	13.0	11.1	7.4	5.3	0.8
Acetone	21.7	23.4	13.0	12.0	11.8	8.7	5.7	0.8
Dimethylacetamide	21.1	23.0	13.6	11.9	10.4	7.4	5.1	0.8
N-Methylacetamide	21.4	22.7	13.4	12.3	10.7	8.2	6.6	0.8
1,3-Dimethylurea	21.5	22.0	12.6	12.1	9.3	7.4	6.3	0.8

TABLE S10 Number of frames for which a given number of geometrically defined HBs to carbonyl oxygens are observed in MD simulations of six solutes in water. These values were used as scaling factors in calculating the ensemble averages of the total electric field as well as the inner- and outer-shell solvent contributions to the field, based on DFT calculations on up to 100 snapshots of a given n_{HB} and solute.

Solute	n_{HB} = 0	n_{HB} = 1	n_{HB} = 2	n_{HB} = 3	n_{HB} = 4
Ethyl Thioacetate	275	2507	2079	140	0
Ethyl Acetate	267	2281	2285	166	2
Acetone	282	2170	2289	259	1
Dimethylacetamide	56	944	3028	959	14
N-Methylacetamide	29	854	2965	1126	27
1,3-Dimethylurea	8	497	2873	1562	61

TABLE S11 Calculated partial charges (in atomic units) on solute carbonyls using Mulliken,[29] AM1-BCC,[30] Merz-Kollman electrostatic potential (ESP),[31-32] or atomic polar tensor (APT)[33] population analyses.

Solute	Mulliken q_C	Mulliken q_O	AM1-BCC q_C	AM1-BCC q_O	ESP q_C	ESP q_O	APT q_C	APT q_O
Ethyl Thioacetate	0.427	-0.398	0.580	-0.533	0.633	-0.493	0.993	-0.757
Ethyl Acetate	0.518	-0.444	0.630	-0.544	0.867	-0.593	1.187	-0.740
Acetone	0.302	-0.429	0.561	-0.531	0.750	-0.551	0.823	-0.698
Dimethylacetamide	0.353	-0.516	0.657	-0.609	0.592	-0.584	1.089	-0.845
N-Methylacetamide	0.362	-0.531	0.657	-0.614	0.660	-0.556	1.075	-0.806
1,3-Dimethylurea	0.441	-0.546	0.728	-0.630	0.928	-0.582	1.339	-0.797

TABLE S12 Calculated dipole moments of the molecule or carbonyl bond using Mulliken, AM1-BCC, Merz-Kollman electrostatic potential (ESP) or atomic polar tensor (APT) partial charges together with the equilibrium bond length, taken from the geometry-optimized structures using DFT at the B3LYP/6-311++G(2d,2p) level. Bond dipoles are calculated with respect to the center of mass of the carbonyl according to $\mu = d\left(\frac{m_O}{m_C+m_O}q_C - \frac{m_C}{m_C+m_O}q_O\right)$, where d is the equilibrium carbonyl bond length (~1.2 Å), m_C and m_O are the atomic masses of carbon and oxygen, respectively, and q_C and q_O are the partial charges on carbon and oxygen, respectively, which are obtained from the various population analyses described.

Solute	Molecular Dipole Moment / D	Mulliken C=O Dipole Moment / D	AM1-BCC C=O Dipole Moment / D	ESP C=O Dipole Moment / D	APT C=O Dipole Moment / D
Ethyl Thioacetate	1.44	2.40	3.27	3.32	5.22
Ethyl Acetate	2.09	2.82	3.47	4.34	5.82
Acetone	3.10	2.07	3.21	3.86	4.50
Dimethylacetamide	3.97	2.48	3.72	3.46	5.76
N-Methylacetamide	3.87	2.54	3.74	3.60	5.61
1,3-Dimethylurea	3.68	2.85	4.01	4.57	6.48

TABLE S13 Calculated partial charge on carbonyl oxygen in water-solvated acetone or *N*-methylacetamide using either a Mulliken or Hirshfeld[34] population analysis at the B3LYP/6-31G(d) level of theory. Note that diffuse basis functions have been removed (from the 6-31+G(d) basis) for these solution-phase calculations due to their tendency to impair the accuracy of population analyses.[35] Average charge on oxygen is calculated for MD simulation frames grouped by number of hydrogen bonds, together with the ensemble averages for the MD trajectories. Ensemble-averaged values are calculated through a weighted average of the results for groups of different n_{HB}, similar to the calculation of the fields in Figure 5C.

n_{HB}	Acetone		*N*-Methylacetamide	
	$q_{O\ (Mulliken)}$	$q_{O\ (Hirshfeld)}$	$q_{O\ (Mulliken)}$	$q_{O\ (Hirshfeld)}$
0	-0.468	-0.215	-0.545	-0.258
1	-0.466	-0.191	-0.548	-0.242
2	-0.475	-0.173	-0.553	-0.218
3	-0.482	-0.160	-0.560	-0.202
4	-0.512	-0.152	-0.572	-0.199
Ensemble avg.	-0.471	-0.183	-0.554	-0.218

TABLE S14 Calculated total charge on the acetone or *N*-methylacetamide solute molecule when solvated in water using either a Mulliken or Hirshfeld[34] population analysis at the B3LYP/6-31G(d) level of theory. Average total solute charge is calculated for MD simulation frames grouped by number of hydrogen bonds, together with the ensemble averages for the MD trajectories. The minimal difference between these two solutes in terms of their ensemble-averaged total charges indicates their similar extents of charge transfer to solvent water molecules.

n_{HB}	Acetone		*N*-Methylacetamide	
	$q_{solute\ (Mulliken)}$	$q_{solute\ (Hirshfeld)}$	$q_{solute\ (Mulliken)}$	$q_{solute\ (Hirshfeld)}$
0	-0.048	0.018	-0.056	0.017
1	-0.019	0.070	-0.043	0.045
2	0.000	0.112	-0.024	0.087
3	0.010	0.137	-0.010	0.122
4	0.058	0.216	-0.008	0.134
Ensemble avg.	-0.010	0.090	-0.025	0.088

TABLE S15 Mean hydrogen bond length for two representative solutes, ethyl thioacetate and 1,3-dimethylurea, in configurations of varying numbers of hydrogen bonds.

Solute	One HB	Two HBs	Three HBs	Four HBs
Ethyl Thioacetate	2.8 Å	2.9 Å	3.0 Å	N.A. (Not observed)
1,3-Dimethylurea	2.7 Å	2.8 Å	2.9 Å	3.0 Å

TABLE S16 Ensemble-averaged hydrogen bond number, $\langle n_{\mathrm{HB}} \rangle$, including 95% confidence intervals, for all six carbonyl-containing solutes in protic solvents.

Solute	Water	Methanol	Chloroform
Ethyl Thioacetate	1.42 ± 0.02	0.79 ± 0.01	0.88 ± 0.02
Ethyl Acetate	1.47 ± 0.02	0.86 ± 0.01	0.91 ± 0.02
Acetone	1.51 ± 0.02	0.83 ± 0.01	0.96 ± 0.02
Dimethylacetamide	1.99 ± 0.02	1.39 ± 0.01	1.41 ± 0.02
N-Methylacetamide	2.05 ± 0.02	1.46 ± 0.01	1.41 ± 0.02
1,3-Dimethylurea	2.23 ± 0.02	1.71 ± 0.01	1.61 ± 0.02

TABLE S17 Decomposition of the overall ensemble-averaged solvent electric field (in MV/cm) for each of the carbonyl-containing solutes obtained using DFT-based calculations, based on the separation of solvents into HB and non-HB ones.

Solute	Hydrogen Bonding Waters Field (MV/cm)	All Non-Hydrogen Bonding Waters Field (MV/cm)	Mutual Polarization of HB- and Non-HB- Waters
Ethyl Thioacetate	-65 ± 3	-25 ± 1	-4.6 ± 0.3
Ethyl Acetate	-66 ± 4	-21 ± 3	-4.4 ± 0.4
Acetone	-65 ± 4	-39 ± 3	-4.1 ± 0.4
Dimethylacetamide	-89 ± 4	-39 ± 3	-5.8 ± 0.6
N-Methylacetamide	-92 ± 4	-47 ± 3	-6.5 ± 0.5
1,3-Dimethylurea	-102 ± 4	-47 ± 3	-7.5 ± 0.5

TABLE S18 Decomposition of the overall ensemble-averaged solvent electric field (in MV/cm) for each of the carbonyl-containing solutes obtained using DFT-based calculations, based on the separation of solvents into those in and out of the first solvation shell.

Solute	Inner-Shell Waters Field (MV/cm)	Outer-Shell Waters Field (MV/cm)	Mutual Polarization of Inner and Outer-Shell Waters
Ethyl Thioacetate	-72 ± 3	-16 ± 3	-5.3 ± 0.5
Ethyl Acetate	-74 ± 3	-13 ± 3	-5.1 ± 0.5
Acetone	-74 ± 2	-29 ± 3	-5.1 ± 0.5
Dimethylacetamide	-95 ± 2	-32 ± 4	-6.4 ± 0.6
N-Methylacetamide	-101 ± 2	-38 ± 3	-7.5 ± 0.6
1,3-Dimethylurea	-107 ± 2	-41 ± 3	-8.3 ± 0.5

IV. Supplemental References

1. Bublitz, G. U.; Boxer, S. G., Stark Spectroscopy: Applications in Chemistry, Biology, and Materials Science. *Annu. Rev. Phys. Chem.* **1997,** *48* (1), 213-242.

2. Fried, S. D.; Bagchi, S.; Boxer, S. G., Measuring Electrostatic Fields in Both Hydrogen-Bonding and Non-Hydrogen-Bonding Environments Using Carbonyl Vibrational Probes. *J. Am. Chem. Soc.* **2013,** *135* (30), 11181-11192.

3. Nelson Jr, R. D.; Lide Jr, D. R.; Maryott, A. A. *Selected values of electric dipole moments for molecules in the gas phase*; National Standard Reference Data System: 1967.

4. Fried, S. D.; Boxer, S. G., Measuring Electric Fields and Noncovalent Interactions Using the Vibrational Stark Effect. *Acc. Chem. Res.* **2015,** *48* (4), 998-1006.

5. Park, E. S.; Boxer, S. G., Origins of the Sensitivity of Molecular Vibrations to Electric Fields: Carbonyl and Nitrosyl Stretches in Model Compounds and Proteins. *J. Phys. Chem. B* **2002,** *106* (22), 5800-5806.

6. Dellepiane, G.; Overend, J., Vibrational spectra and assignment of acetone, ααα acetone-d3 and acetone-d6. *Spectrochim. Acta* **1966,** *22* (4), 593-614.

7. Schneider, S. H.; Kratochvil, H. T.; Zanni, M. T.; Boxer, S. G., Solvent-Independent Anharmonicity for Carbonyl Oscillators. *J. Phys. Chem. B* **2017,** *121* (10), 2331-2338.

8. Bagchi, S.; Fried, S. D.; Boxer, S. G., A Solvatochromic Model Calibrates Nitriles' Vibrational Frequencies to Electrostatic Fields. *J. Am. Chem. Soc.* **2012,** *134* (25), 10373-10376.

9. Liptay, W., Electrochromism and solvatochromism. *Angew. Chem. Int. Ed.* **1969,** *8* (3), 177-188.

10. Liptay, W., Dipole moments and polarizabilities of molecules in excited electronic states. In *Excited states*, Elsevier: 1974; Vol. 1, pp 129-229.

11. Carr, J. K.; Zabuga, A. V.; Roy, S.; Rizzo, T. R.; Skinner, J. L., Assessment of amide I spectroscopic maps for a gas-phase peptide using IR-UV double-resonance spectroscopy and density functional theory calculations. *J. Chem. Phys.* **2014,** *140* (22), 224111.

12. Schneider, S. H.; Boxer, S. G., Vibrational Stark Effects of Carbonyl Probes Applied to Reinterpret IR and Raman Data for Enzyme Inhibitors in Terms of Electric Fields at the Active Site. *J. Phys. Chem. B* **2016,** *120* (36), 9672-9684.

13. Böttcher, C. J. F., *Theory of Electric Polarization*. 2nd ed.; Amsterdam, 1973; Vol. 1.

14. Bublitz, G. U.; Boxer, S. G., Effective Polarity of Frozen Solvent Glasses in the Vicinity of Dipolar Solutes. *J. Am. Chem. Soc.* **1998,** *120* (16), 3988-3992.

15. Choi, J.-H.; Oh, K.-I.; Lee, H.; Lee, C.; Cho, M., Nitrile and thiocyanate IR probes: Quantum chemistry calculation studies and multivariate least-square fitting analysis. *J. Chem. Phys.* **2008,** *128* (13), 134506.

16. Miller, T. M., Polarizabilities of Atoms and Molecules. In *CRC Handbook of Chemistry and Physics*, 102nd Edition (Internet Version 2021) ed.; Rumble, J. R., Ed. CRC Press/Taylor & Francis: Boca Raton, FL.

17. Zheng, C.; Mao, Y.; Kozuch, J.; Atsango, A. O.; Ji, Z.; Markland, T. E.; Boxer, S. G., A two-directional vibrational probe reveals different electric field orientations in solution and an enzyme active site. *Nat. Chem.* **2022**.

18. Max, J.-J.; Chapados, C., Infrared spectroscopy of acetone-hexane liquid mixtures. *J. Chem. Phys.* **2007,** *126* (15), 154511.

19. Schweitzer-Stenner, R.; Sieler, G.; Christiansen, H., Competition between peptide-peptide and peptide-solvent hydrogen bonding probed by polarized Raman spectroscopy on N-methylacetamide. *Asian J. Phys.* **1998,** *7*, 287-312.

20. Vargas, R.; Garza, J.; Friesner, R. A.; Stern, H.; Hay, B. P.; Dixon, D. A., Strength of the NH···OC and CH···OC Bonds in Formamide and N-Methylacetamide Dimers. *J. Phys. Chem. A* **2001,** *105* (20), 4963-4968.

21. Choi, J.-H.; Cho, M., Vibrational solvatochromism and electrochromism of infrared probe molecules containing C≡O, C≡N, C=O, or C−F vibrational chromophore. *J. Chem. Phys.* **2011,** *134* (15), 154513.

22. Choi, J.-H.; Oh, K.-I.; Cho, M., Azido-derivatized compounds as IR probes of local electrostatic environment: Theoretical studies. *J. Chem. Phys.* **2008,** *129* (17), 174512.

23. Weaver, J. B.; Kozuch, J.; Kirsh, J. M.; Boxer, S. G., Nitrile Infrared Intensities Characterize Electric Fields and Hydrogen Bonding in Protic, Aprotic, and Protein Environments. *J. Am. Chem. Soc.* **2022,** *144* (17), 7562-7567.

24. Kozuch, J.; Schneider, S. H.; Zheng, C.; Ji, Z.; Bradshaw, R. T.; Boxer, S. G., Testing the Limitations of MD-Based Local Electric Fields Using the Vibrational Stark Effect in Solution: Penicillin G as a Test Case. *J. Phys. Chem. B* **2021,** *125* (17), 4415-4427.

25. Zaiontz, C. *Real Statistics Resource Pack*, real-statistics.com: 2022.

26. DeCamp, M. F.; DeFlores, L.; McCracken, J. M.; Tokmakoff, A.; Kwac, K.; Cho, M., Amide I Vibrational Dynamics of N-Methylacetamide in Polar Solvents: The Role of Electrostatic Interactions. *J. Phys. Chem. B* **2005,** *109* (21), 11016-11026.

27. Luzar, A.; Chandler, D., Structure and hydrogen bond dynamics of water–dimethyl sulfoxide mixtures by computer simulations. *J. Chem. Phys.* **1993,** *98* (10), 8160-8173.

28. Maibaum, L.; Chandler, D., Segue between Favorable and Unfavorable Solvation. *J. Phys. Chem. B* **2007,** *111* (30), 9025-9030.

29. Mulliken, R. S., Electronic Population Analysis on LCAO–MO Molecular Wave Functions. I. *J. Chem. Phys.* **1955,** *23* (10), 1833-1840.

30. Jakalian, A.; Jack, D. B.; Bayly, C. I., Fast, efficient generation of high-quality atomic charges. AM1-BCC model: II. Parameterization and validation. *J. Comput. Chem.* **2002,** *23* (16), 1623-1641.

31. Singh, U. C.; Kollman, P. A., An approach to computing electrostatic charges for molecules. *J. Comput. Chem.* **1984,** *5* (2), 129-145.

32. Besler, B. H.; Merz Jr, K. M.; Kollman, P. A., Atomic charges derived from semiempirical methods. *J. Comput. Chem.* **1990,** *11* (4), 431-439.

33. Cioslowski, J., A new population analysis based on atomic polar tensors. *J. Am. Chem. Soc.* **1989,** *111* (22), 8333-8336.

34. Hirshfeld, F. L., Bonded-atom fragments for describing molecular charge densities. *Theor. Chim. Acta* **1977,** *44* (2), 129-138.

35. D. Thompson, J.; D. Xidos, J.; M. Sonbuchner, T.; J. Cramer, C.; G. Truhlar, D., More reliable partial atomic charges when using diffuse basis sets. *Phys. Chem. Comm.* **2002,** *5* (18), 117-134.